LAPPEENRANTA UNIVERSITY OF TECHNOLOGY
Faculty of Technology
Master's Degree Program in Technomathematics and Technical Physics

Natalia Nikitina

Magnetic sputtering of complex oxides

Examiners: Professor Erkki Lähderanta
PhD Vladimir T. Barchenko

ABSTRACT

Lappeenranta University of Technology
Faculty of Technology
Master's Degree Program in Technomathematics and Technical Physics

Natalia Nikitina

Magnetic sputtering of complex oxides

Master's thesis

2010

42 pages, 22 figures, 3 tables, 2 appendices

Examiners: Professor Erkki Lähderanta
PhD Vladimir T. Barchenko

Keywords: magnetic sputtering, producing HTS, modeling physical processes

HTSC materials are relevant in modern microelectronics, because of their transformation from the normal state to the superconducting. That is why the idea of producing HTSC in industrial amounts is actual nowadays. To decrease cost of their production it is important to use magnetron sputtering systems which give the best results for essential parameters. Modeling is the simplest and the fastest way to determine optimum sputtering condition.

This thesis concentrates on determination the phases of the whole sputtering process and to find out basic factors of each phase using the modeling. It was find out, that the main factors which influence on the mode of occurrence of the initial stages are the current density of the magnetron discharge and the pressure of sputtering gas. With the modeling also velocity dependences were obtained for YBCO and SmFeAsO. These were compared and difference between them was examined. To support represented model comparison was made with experimental results. This showed that the model gives good results, very similar to the experimental ones.

The results of this work were published in annual conference of the finnish physical society.

ACKNOWLEDGEMENTS

I would like to thank Professor E. Lahderanta, PhD V. T. Barchenko and Professor S. F. Karmanenko for the advices and guidance that I have received during the writing process. I wish to present a special acknowledgement to my parents and to my friends who have supported and encouraged me during my studies and thesis work.

TABLE OF CONTENTS

LIST OF ABBREVIATIONS

ADC	analog-to-digital converter
ADD	area of the diffusion distribution of sputtered atoms
CDS	cathode dark space
EBE	electron-beam evaporation
HTSC	high temperature superconductors
I-V	current-voltage characteristic
LE	laser evaporation
LSC	the laboratory system of coordinates
MOCVD	method of gas-phase deposition of organ metallic compounds
MS	magnetron sputtering
MSS	magnetron sputtering system
PC	positive column
RES	region of elastic scattering
RT	region of thermalization
UDFT	uniform distribution of the film thickness
YBCO	superconductor $YBa_2Cu_3O_7$

1. Introduction

All superconductors can be classified by the critical temperature *Tc*, temperature of the transition from the normal (when the substance is non-zero electrical resistance) to the superconducting state. Superconductors with high *Tc* are called high-temperature superconductor (abbreviated as HTSC) and with a low *Tc* are called low temperature superconductors. The boundary between them passes the junction Nb_3Ge with a critical temperature of approximately 23 K.

1.1 History of discovery

In 1987, Johannes Georg Bednorz and Karl Alex Muller discovered the first high-temperature superconductors, $La_{2-x}Ba_xCuO_4$. It was clear that the BCS theory of superconductivity was not able to explain the high critical temperature of this compound. After $La_{2-x}Ba_xCuO_4$ the same puzzle represented and other high-temperature superconductors with higher *Tc*.

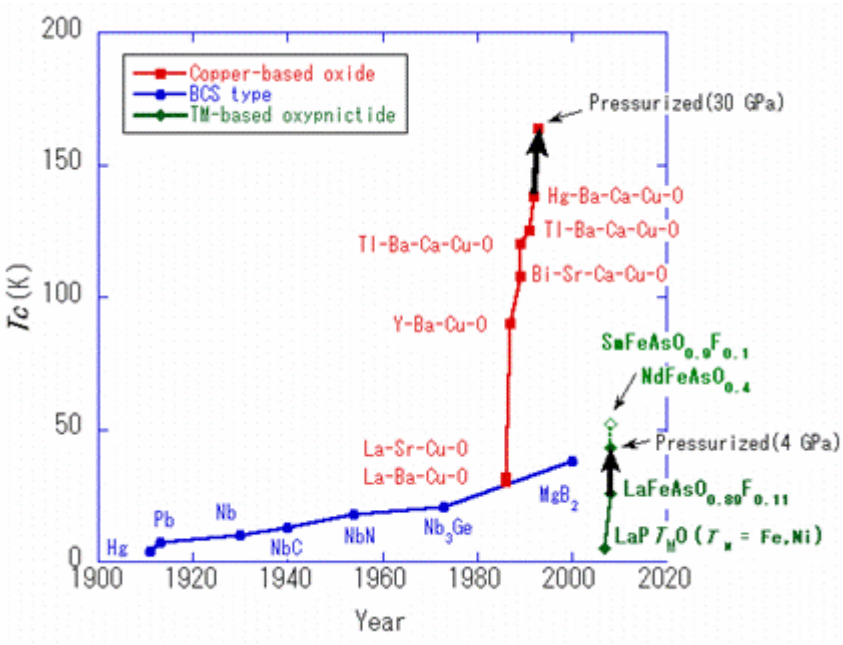

Fig. 1.1.1. Timeline of discovery of superconducting materials. Some important dates:

1911 - first observation on the phenomenon of superconductivity of mercury by Kamerlingh Onnes;

1986 - Opening of the first high-temperature superconducting materials, ceramics based on lanthanum, barium and copper oxide;

1987 - Chu and others synthesize material $YBa_2Cu_3O_{7-x}$ with a critical temperature 93 K, i.e. above the boiling point of nitrogen;

January 1988 - Maeda et al observed *Tc* = 108 K in conjunction $Bi_2Sr_2Ca_{n-1}Cu_nO_{2n-4}$ (n = 3);

February 1988 - Sheng and Herman got $Tl_2Ba_2Ca_2Cu_3O_{10}$ superconductor with *Tc* = 125 K;

1993 - Antipov, Putilin etc. opened a number of mercury-containing superconductors $HgBa_2Ca_{n-1}Cu_nO_{2n+2+d}$ (n = 1 - 6).

Currently, phase $HgBa_2Ca_2Cu_3O_8$ has the highest known value of the critical temperature (135 K), and under external pressure, of 350 thousand atmospheres, the transition temperature increases to 164 K, which is only 19 degrees to the lowest temperature recorded in natural conditions on Earth.

2008 - The opening of the first iron-containing high-temperature superconducting material [26].

1.2 Areas of application

Currently, many laboratories in the world are involved in developing of cryoelectronic devices and devices based on superconducting films.

The establishment of specific technical products based on HTSC materials most effectively in the near future is in the low-current technique, such as in microelectronics and computer technology.

The widespread use of HTSC found in computer science. It was developed, manufactured and tested models of memory cells, hypersensitive element of the readout on the HTS films with multiple lower energy compared to solid-state amplifier readout, high-speed communication lines, that will increase the performance of systems in 10 – 100 times.

One of the promising areas of HTSC is space technology with inside and outside instrumentation and computer systems. This can work without special cooling devices, as the “shadow” temperature at the satellite is 90 K. Wide possibilities prospects of HTSC open in microwave technology and the creation of sensors of visible and infrared range with high sensitivity.

Application of HTSC in high-technology will have the most drastic economic consequences for the economy. This area includes the creation of electric devices and systems for generating, transmitting and transforming electricity to industrial scale. The basis of this trend is the ability of superconductors to carry no loss of high-density transport current (10^9 - 10^{10} A/m^2) in strong magnetic fields at temperatures below the critical. This property of superconductors can create electrical power equipment for various purposes with improved weight and size characteristics, higher efficiency and significant (up to ten times) reduction in operating costs. Superconducting inductive energy storage will have a much higher efficiency, up to 97-98% instead of 70%.

There are superconducting separators, NMR tomography, and magnetic systems for plasma confinement in Tokamak and particle accelerators, etc. Creation of such systems will provide the necessary technical and technological basis for a rapid transition to high-temperature superconductors as creating technology-based HTSC conductors.

1.3 Structure and electrical properties of high temperature superconductors

1.3.1.YBCO

During of physics, chemistry and technology of HTSC oxide materials, a series of new compounds and their films were obtained by different technological methods. La-Ba-Cu-O with orthorhombic structure and the critical temperature superconducting transition, *Tc* ≈ 40 K, was the first oxide in a continuously growing number of HTSC materials. Very promising family of materials is Ti-and Bi-superconductors with superconducting transition temperature above 100 K. At the same time, the formation of superconducting films, which contains Ti, Bi, meets many difficulties such as complicated phase diagram and phase structure.

The most studied high-temperature superconducting (HTSC) is the connection metal-oxide $YBa_2Cu_3O_{7-\delta}$ with the structure of perovskite-type orthorhombic 1-2-3 phase. This has a critical temperature of superconducting transition *Tc* ≈ 90 K. Compound $YBa_2Cu_3O_{7-\delta}$ has a unit cell with parameters *a* = 3.824 Å, *b* = 3.894 Å, *c* = 11.683 Å. The parameter *a* is almost identical with *b* and parameter *c* is approximately three times *b*. Schematic representation of the elementary lattice $YBa_2Cu_3O_{7-\delta}$ is presented in Figure 1.3.1.

Type of conductivity, the critical temperature of superconducting transition, the critical current density strongly depend on oxygen content The most high concentration of oxygen in the lattice $YBa_2Cu_3O_{7-\delta}$ are the values of δ = 0.05 - 0.2. [1]

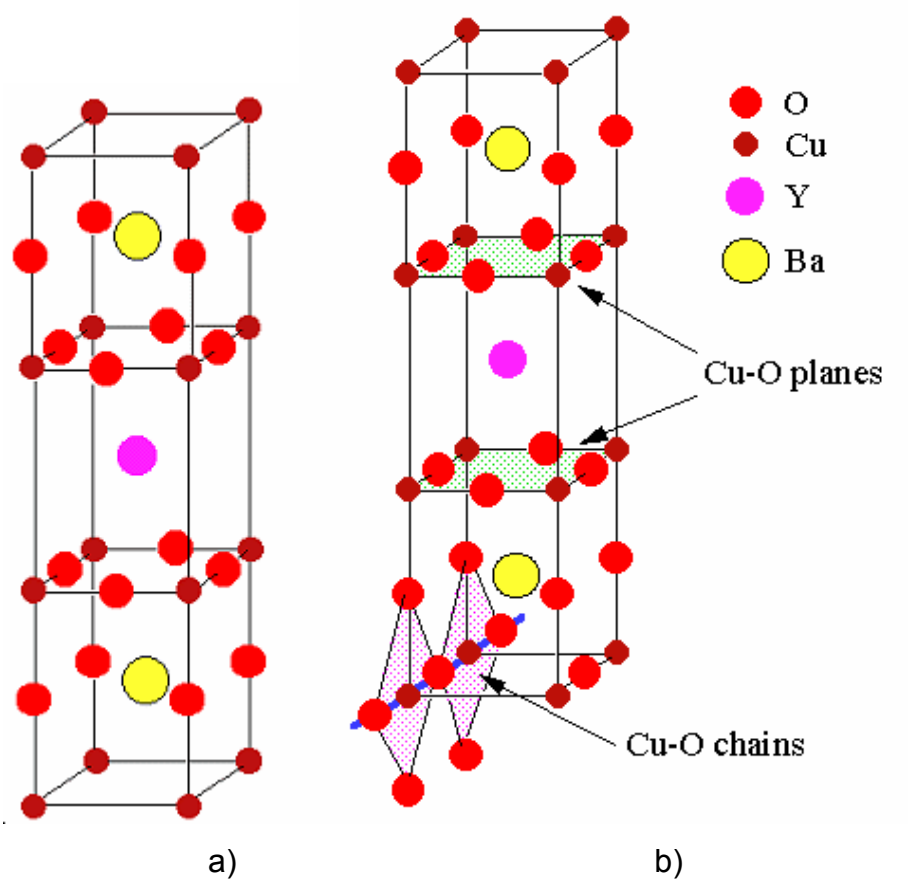

Fig. 1.3.1. Elementary crystal lattice of HTSC compounds $YBa_2Cu_3O_{7-\delta}$, a) $YBa_2Cu_3O_6$, b) $YBa_2Cu_3O_7$ [25].

1.3.2. Iron-based superconductors

For a long time it was believed that all the unusual high-temperature superconductors contain copper in its composition. Because of that, they are often called copper-bearing, or cuprates. February 23, 2008, a group of Japanese scientists led by Hideo Hosono [5] described superconductivity in LaF_xFeAsO_{1-x} (x = 0.05 – 0.12) with *Tc* = 26 K. It became clear that the HTSC could include also some iron-containing substances.

At the moment, superconductivity was found in four classes of iron-containing compounds: ReFeAsO (Re is rare earth metal), $AeFe_2As_2$ (Ae is alkaline earth metal), AFeAs (A is alkaline metal) and FeCh (Ch is chalcogen). The maximum critical temperature of 56 K was achieved for GdFeAsO.

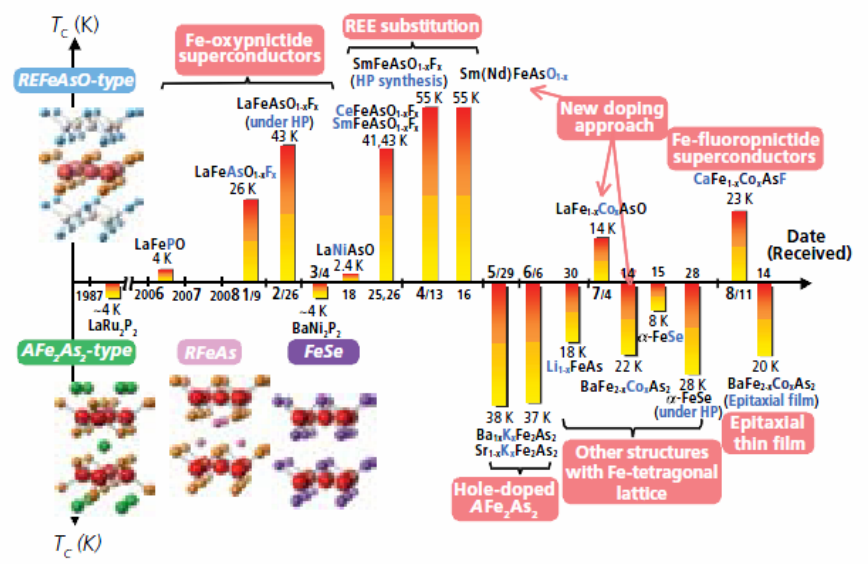

Fig.1.3.2. Development of iron-based superconductors [2].

All iron-pnictide superconductors include two-dimensional (2-D) Fe*Pn* (*Pn* is: pnictogen atom) layers with a tetragonal structure at room temperature, which is shown in Fig. 1.3.3. Therefore, their physical properties are considered to be highly two-dimensional, similarly to those cuprates, ruthenate and cobaltate superconductors.

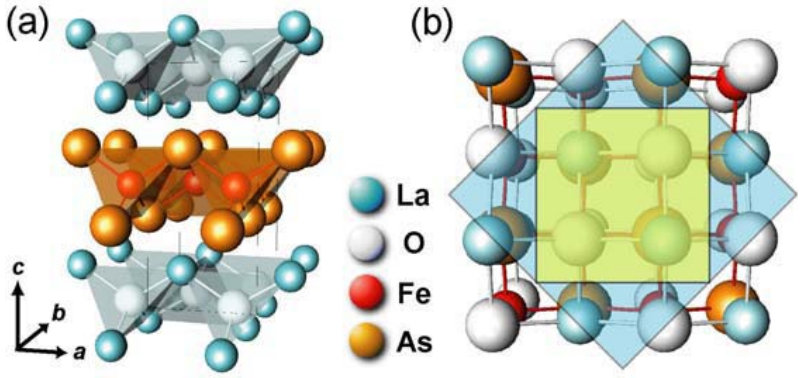

Fig. 1.3.3. Crystal structure of LaFeAsO. (a) Schematic image of the crystal lattice shows a layered structure. Disorted tetrahedrons $FeAs_4$, connected at the edge sharing manners, form the FeAs layer. (b) Top view of the crystal structure in the c-orientation [6].

Table 1. shows the critical temperature for different elements and the amount of oxides on them (x). This shows the best result in the field of achieving the highest superconducting transition temperature.

Table. 1. The maximum Tc in each RFeAs ($O_{1-x}F_x$). The concentration of F_x, which gives the highest T_c, is shown. T_{cmax} is defined as the superconducting transition temperature [7].

R	*La*	*Ce*	*Pr*	*Nd*	*Sm*	*Gd*	*Tb*	*Dy*
T_{cmax}*[K]*	28	41	52	52	55	36	46	45
x	0.11	0.16	0.11	0.11	0.1	0.17	0.1	0.1

In iron-based superconductors, containing fluorine temperature dependence of resistivity looks has T^2. But for those, that don't have F, there is no T^2 dependence observed. Fig. 1.3.4 shows the temperature dependence of electrical resistivity. ρ is roughly proportional to temperature down to 200 K, and shows a downward curvature at approximately 150 K.

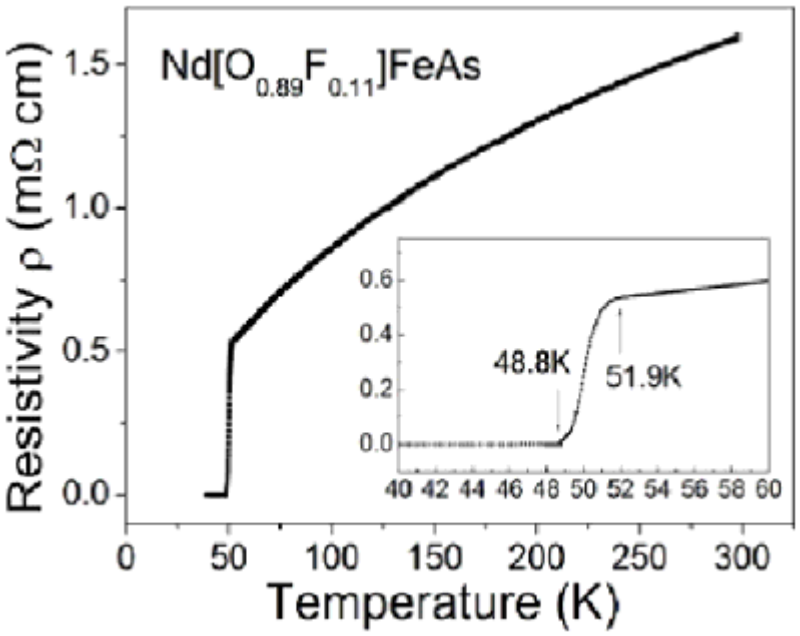

Fig.1.3.4. Temperature dependence of electrical resistance for NdFeAs ($O_{0.89}F_{0.11}$). [7]

As stated above, the resistance of undoped LaFeAsO and $BaFe_2As_2$ has abnormal behavior at T approximately 150 K, which refers to the magnetic and structural changes.

1.4. Achievements in technology for HTSC

At this point, all the technology of oxide films can be divided into two main areas [8]:

- Physical methods, in which the flow of particles on the substrate is created by physical processes. They are evaporation, sputtering, and the formation of the film occurs in the interaction of the components of the desired compound;
- Chemical methods, which are used as sources of complex chemical compounds, mostly, organometallic, and the process of transfer of atoms occurs in the form of complex chemical compounds, recovering in the zone of condensation of the film, and restored the atoms form the desired compound on the substrate.

Major achievements for the films are related to physical methods, at the moment associated with physical methods to obtain [9-10]. But also, there is active development of the method of gas-phase deposition of organometallic compounds (MOCVD). [11] This method allows to obtain films with high critical parameters and oriented structure with film thickness of 7...10 nm. Nevertheless, the limiting critical characteristics of high-temperature superconducting films of YBCO are Tc = 92 K and $Jc = 7 * 10^6$ A/cm^2 [12] for films obtained by laser evaporation and magnetron sputtering. The superconducting films prepared by laser evaporation show critical parameters inferior than the films grown by magnetron sputtering. This is probably due to the fact that laser vaporization gives films with mixed orientation, undesired for superconductors. Development and implementation of the method of MOCVD has serious drawbacks associated with a large percentage of material that differs from the stoichiometry. Therefore, for producing high-temperature superconductors are used mainly physical methods: laser ablation and magnetron sputtering, in connection with a good quality of the films and the relative simplicity of their receipt.

Electron-beam evaporation (EBE) is performed by heating the source material by focused stream of high-energy electrons. The main advantage of the method EBE is high precision process control and the ability to grow layer by layer. For HTSC, this method is rarely used in connection with what is needed is extremely saturated with

oxygen grown structure and complexity of building «in-situ» of the process of formation. The main disadvantage of this process is great difficulty in obtaining homogeneous films on the properties of extended surfaces.

Laser evaporation (LE) is used in continuous and pulsed modes. The main advantage of this method is good evaporation of all chemical elements. LE also allows good control over stoichiometry to produce films, as well as the basic parameters of the evaporation process. The most important parameters of the method of evaporation are the distance from the target to the substrate and the oxygen pressure. LE helps to reduce heating of the substrate. Hence it reduces the number of radiation-induced defects. The latter may include a small area of deposition, the roughness of the film obtained, as well as the thickness of the surface roughness.

Magnetron sputtering (MS) is the most common method for obtaining high-temperature superconductors. The popularity is because it is sufficient easy to make of installation. One can get the film with the required stoichiometry, low roughness and fairly uniformly over the thickness. The advantages of this method include good reproducibility of the process and parameters of the system under which the spraying is carried out. Consideration should be given more careful.

2. Magnetron Sputtering

Magnetron sputtering system (MSS) got its name from the microwave devices of M-type (magnetron devices). The only connection to it is the presence of crossed electric and magnetic fields. Magnetron systems are systems such as diode sputtering, in which the sputtering material is due to the bombardment of the target surface ions of the working gas, formed in the gas abnormally glow.

2.1. Basic physical processes in MSS

Design of the MSS includes a cathode-target of the spray material, a water cooling system of the target and the magnetic system. MSS scheme is shown in Fig.2.1.1.
When a constant voltage is applied between the target (negative potential) and the anode (positive potential) there is a nonuniform electric field. In the working zone of the electric field is perpendicular to the magnetron and the magnetic field tangential to the surface of the cathode target. The values of the magnetic field are in the range 30 - 150 mT. The plasma is magnetized and the ions are practically not influenced by the magnetic field. When using MSS, the electrons drift parallel to the target by closed

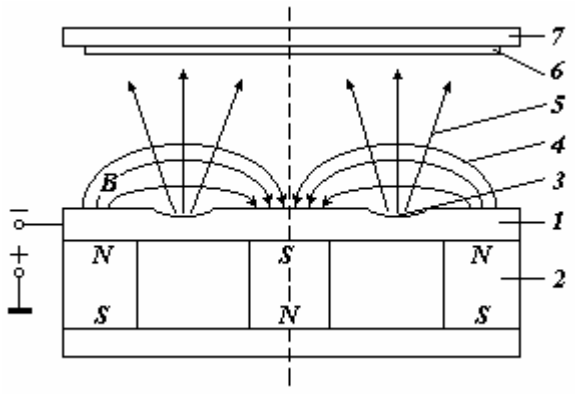

Fig. 2.1.1. Scheme of the magnetron sputtering system:
1 is target, 2 is magnetic system, 3 is zone spray,
4 are magnetic field lines; 5 is flow of sputtered
material, 6 is substrate; 7 is substrate. [4]

cycloidal trajectories. On average, a single collision of the electron is shifted in the direction of the electric field at a distance of order the Larmor's radius R_L (called the Larmor's circle, on which the particle moves in a transverse magnetic field). In this connection, the Larmor's radius of the magnetron sputtering system (MSS) starts to play a role similar to the mean free path in the discharges without magnetic field. Since the R_L of the electrons in the MSS is rather small, of the order of 1 mm, fast free electrons are locked in a trap near the cathode surface. So they can only waste their energy in collisions, including and lead to ionization.

Magnetron sputtering refers to methods of ion-plasma sputtering. The basis of this method is the presence of crossed electric and magnetic fields. In the non-uniform crossed electric and magnetic fields, charged particles perform drift. Although consideration of the drift motion of individual particles is not enough for a complete description of the plasma, they can be graphically describe some macroscopic properties of the plasma state.

Electron trajectory in the plasma of MSS systems is very complex, and it is impossible to describe it analytically. The quantitative determination of the complex motion of charged particles in a gas is expanded into two components: random (diffusion) and directed movement. The predominance of a particular type of motion depends on the gas pressure p and the electric field E, acting in the discharge. The criterion for assessing the nature of particles is the ratio of E / p. If this parameter is large, the predominant direction is the direction of an electric field. In magnetron sputtering systems there are space charges and small field of cathode and anode potential drop, which are characterized by high electric field, the value of E / p is greater than 10^5 V / m * Pa, which makes the motion of electrons directed.

Due to strong differences between the masses of ion and electron impact on the character of the motion, the magnetic field influences only on electron's motion. Magnetizing of an electron leads to the fact that electrons are in a magnetic trap near the target. Because of this effect the temperature load decreases on the substrate, and radiation effects decrease.

A special feature of magnetron sputtering systems is the localization of abnormal plasma glow discharge in sputtering targets, and the plasma has a shape close to the toroidal. The degree of ionization is maximal in the central part of the spray zone. The

reason for the localization of plasma on the middle zone of sputtering is in the inhomogeneity of the magnetic and electric fields.

The magnetic field exerts a strong influence on the parameters and structure

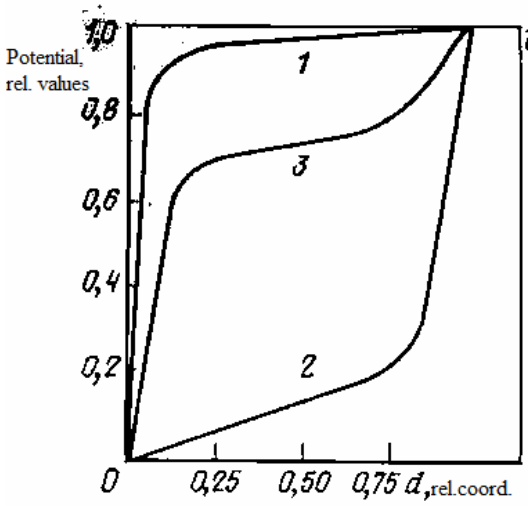

Fig. 2.1.2. Potential distribution in the discharge gap with MSS cylindrical electrodes [4].

of discharge. Since the movement of ions in the plasma is weakly dependent on magnetic fields, the mobility of electrons across the magnetic field is significantly lower than that of ions. At the anode forms a negative space charge and the anode layer is formed, which is the anode potential drop. For sufficiently large magnetic field, almost all the applied voltage may drop in the anode layer. Electrons are accelerated in this field and ionize the gas atoms. This results in the dominant ionization of the anode region, and the thickness of the anode layer is a function of magnetic field. Thus, in the case of crossed electromagnetic fields 3 types of dependence on the magnitude of the magnetic field can be observed: the discharge from the cathode fall, the discharge from the anode fall and level with the simultaneous existence of both regions (Fig. 2.1.2).

2.2. Main dependences of the most important parameters

One of the main characteristics of the discharge is a current-voltage characteristic (I-V). The working pressure (p) and magnetic induction (B) have significant influence on it.

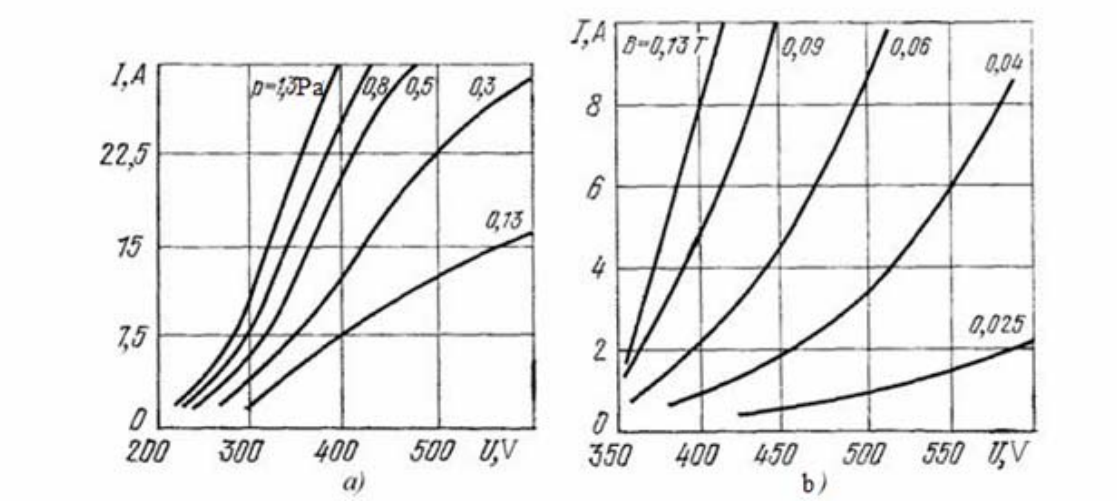

Fig. 2.2.3. Current-voltage characteristics of magnetron sputtering systems: a) with an aluminum target size of 40x60 cm with a constant magnetic field of 0.03 T at various pressures of argon, b) with an aluminum target with a diameter of 160 mm at a constant argon pressure of 0.3 Pa and varying the magnetic field [4].

With decreasing *p* I-V shifted to higher operating pressures and becomes closer to linear dependence (see Figure 2.2.3 a). Almost the same effect gives the magnetic field (see Figure 2.2.3 b). Similar to the linear dependence is observed at large values of *B*. At the I-V of the discharge is also influenced by the target material (see Figure 2.2.4 a) and its shape, which varies with the sputtering material. Education gap in the plane of the target leads to a shift toward lower I-V operating voltage due to the improvement of the localization of the plasma, and this shift increases with increasing p (see Figure 2.2.4. b). In this case, the determining factor is not only the geometric factor, but also the transition of the discharge zone in the region of strong magnetic field as the sputtering target.

An important parameter of discharge determining the rate of sputtering is the electric power, and the rate of deposition of the film is almost linearly depending on the applied power. (See Fig. 2.2.5. a) [10]. In turn, the power level at a constant power source depends on *p* and *B*. In sufficiently weak magnetic fields there is a value *p*, at which the discharge allocate the maximum power (see Fig. 2.2.5. b). With an increase (up to 0.04 T) at low values of *p,* power level initially rises sharply, then goes slowly down and at B = 0,08 - 0,1 T is the maximum. At sufficiently high *p* the maximum power achieved already at B = 0, 04 - 0,06 T (see Fig.2.2.6.a).

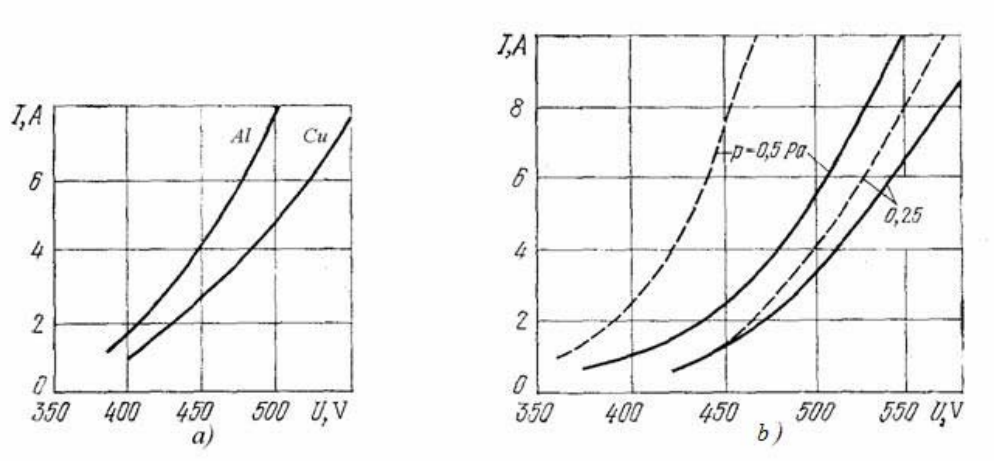

Fig. 2.2.4. I-V characteristics of the magnetron sputtering system: a) with a flat target made of various metals at constant pressure 0.5 Pa. and magnetic induction 0.08 T, b) with a conical new (solid line) and eroded (dashed lines) targets in the magnetic induction 0.06 T and different pressures [4].

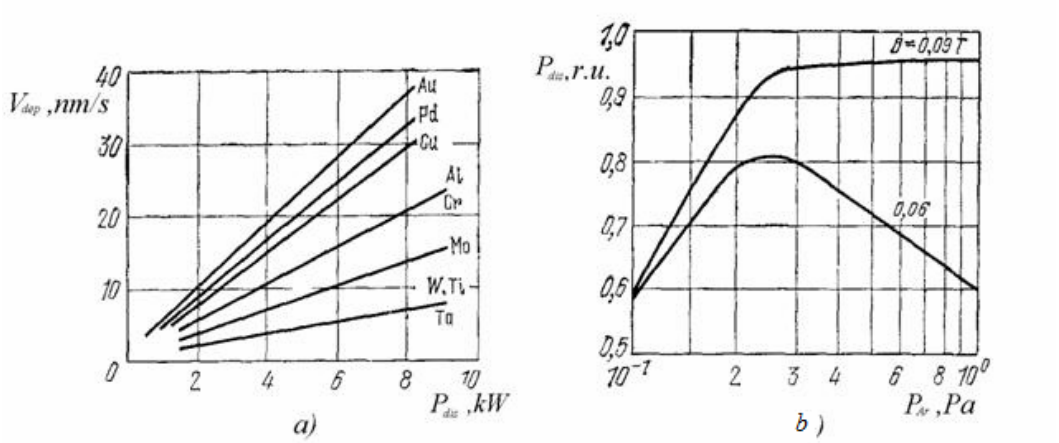

Fig. 2.2.5. Dependence of the rate of deposition of various materials from the discharge power (a) and discharge power on the working pressure at different magnetic induction (b) [4].

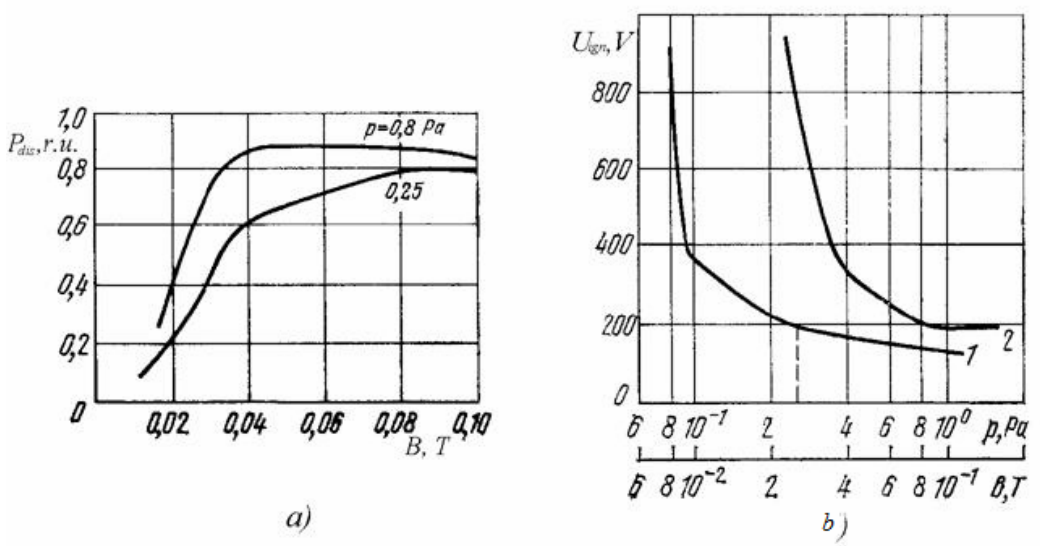

Fig. 2.2.6. Dependence of the power level of the magnetic field at various pressures of argon (a), and the ignition voltage of the pressure at constant magnetic induction 0.06 T (curve 1) and the magnetic field at constant pressure (curve 2) (b) [4].

Ignition voltage in a magnetron system is much lower than in conventional diode systems. Before the imposition of an electric field, the electrons always presents in the volume of the system and provides the first acts of ionization. Resulting is that their concentration in this area is higher than in the volume that contributes to the discharge at lower voltages. It was shown that the dependence of the firing voltage of the pressure of working gas and the magnetic field are similar (see Figure 2.6.b). The similarity of the curves presented points to the fact that the magnetic field and the working pressure have the same effect on the emergence and development of the discharge in MSS.

The required rate of deposition in a magnetron system with sufficient accuracy can be maintained through constant process parameters such as discharge current or input power. These functions can execute a power supply, so one can manage the final film thickness, if the time of deposition is given. However, you can control the growth of the film with the help of direct control methods, such as a quartz sensor, since the plasma in the magnetron system is localized and does not affect the sensor. In practice, to ensure repeatability and stability of the film deposition process the discharge current must maintain within ± 2%, while stabilization of the discharge power to maintain its accuracy is ± 20 W in the control range of 0 to 10 kW. The working pressure must be constant; deviation must not exceed ± 5%.

The deposition rate at a given point of the substrate depends not only on the emission characteristics of the source, but also from the spray, condensation angles φ, ψ and distance between the sputtering points r. A characteristic feature is the presence of MSS in the target narrow band spraying, generally shaped like a ring or elongated ellipse, which greatly complicates the problem of radiation film on a substrate with the desired uniformity in thickness. To increase the uniformity of deposition are two ways. The first way is derived from the thermal vacuum deposition method provides a planetary rotation during the deposition of films for them, resulting in angle of incidence of atoms sputtered material on the receiving surface of the substrate on is constantly changing. Second way to increase the uniformity of deposition provides for optimizing the geometry of the MSS and its spatial location at which the high uniformity can be achieved with a stationary or linear displacement on a rotating MSS substrate [13].

2.3. Simulation of the distribution of coating thickness on the Danilin's model

The simulation of the distribution of coating thickness on the Danilin's model. During the simulation process MSS will be treated with flat cathode. It should be noted that essentially only in the initial moment of sputtering ions bombard the flat target. Subsequently the target is subjected to bombardment of the surface with a V-shaped profile, the depth of which increases continuously. As the degree of erosion of the target rate

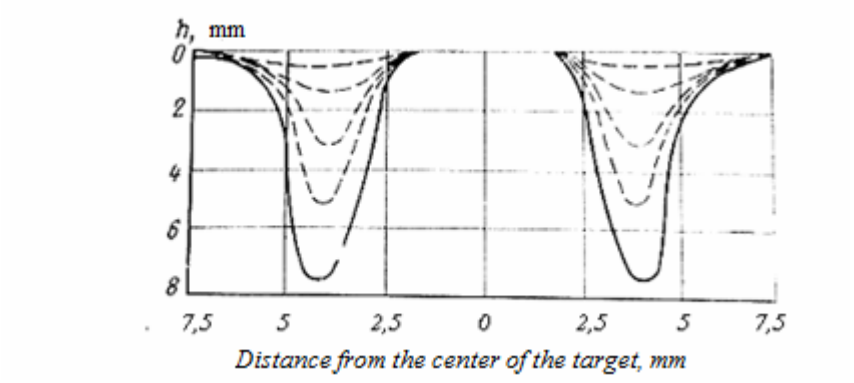

Fig. 2.3.1. Changing the zone of erosion of a planar magnetron with a circular target in the sputtering process [4].

deposition of sputtered material is reduced; the change in deposition rate depends on the design of the MSS and the discharge current. Reducing the deposition rate can be compensated for increasing duration of the deposition process. The accuracy of the correction mode of deposition can be significantly enhanced in the case of known experimental curve of the deposition rate of the operating time of the target at a fixed discharge current.

Danilin's model of flat annular evaporator is a special case of the model for a conical evaporator (in this case, the angle of taper of the target is zero).

Assume that the mean free path of evaporated atoms is not less than the distance from the cathode to the substrate (direct-flight mode), the distribution of material in space is on the cosine law; the velocity distribution is proportional to the ion current density.

A characteristic feature of MSS is the presence of a narrow zone at the target sputtering (Fig. 2.3.1.). Usually a ring-shaped, or elongated ellipse, greatly complicates the problem of obtaining a film on a substrate with the desired uniformity in thickness.

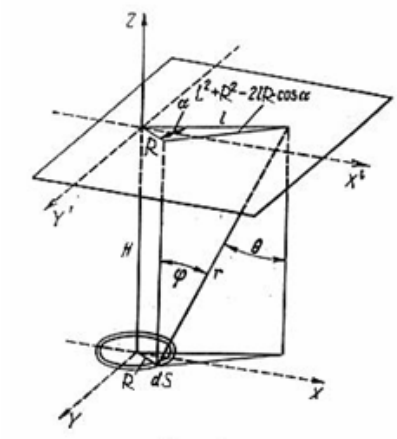

Fig. 2.3.2. Sputtering elements of a flat disk evaporator element substrate [4].

Introduce the following notation:

l the width of the annular zone sputtering;

Rp the distance from the point of condensation to the center of the substrate;

N the average distance from the substrate to the target;

α the polar angle;

γ the angle of taper of the target (in this case γ = 0);

R radius of the current target.

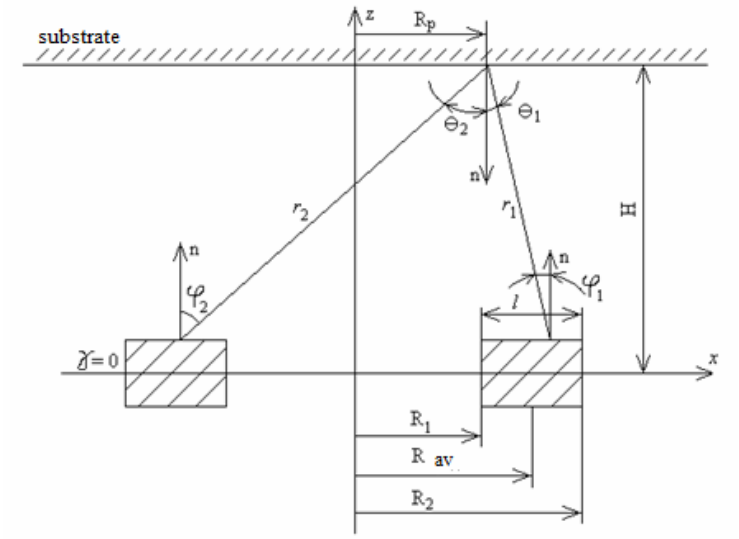

Fig. 2.3.3. Basic geometrical relations that characterize the magnetron system with a target in the form of a flat ring [4].

When the target has the shape of body rotation, on its surface there is a narrow annular zone width *l* with inner and outer radiuses R_1 and R_2 (Fig. 2.3.3) , respectively, of geometric constructions It should following equations (2.3.1):

$$\begin{aligned} &H_1 = H + (R_2 - R)tg\gamma; \\ &\cos\varphi(R,\alpha) = \tfrac{1}{r}\left[H_1\cos\gamma + \left(R - Rp\cos\alpha\right)\sin\gamma\right]; \\ &\cos\theta(R,\alpha) = \frac{H_1}{r}; \\ &r(R,\alpha) = \left(H_1^2 + R_P^2 + R^2 - 2R_pR\cos\alpha\right)^{\frac{1}{2}} \end{aligned} \quad . \qquad (2.3.1)$$

The general formula for calculating the thickness of the film in this case is:

$$h(R_p) = \int_{R1}^{R2}\int_{0}^{2\pi} \frac{\cos\varphi(R,\alpha)\cos\theta(R,\alpha)R\cdot\Pi(R)}{r^2(R,\alpha)\cos\gamma} d\alpha\, dR \quad . \qquad (2.3.2)$$

In this case, the angle of taper of the target is zero. With this in mind, we rewrite these expressions, substituting them $\gamma = 0$. Then:

$$H_1 = H + (R_2 - R)tg\,0 = H;$$

$$\cos\varphi(R,\alpha) = \frac{1}{r}\left[H_1\cos\gamma + (R - Rp\cos\alpha)\sin\gamma\right] = \frac{1}{r}\left[H\cos 0 + (R - Rp\cos\alpha)\sin 0\right] =$$

$$= \frac{1}{r}\left[H + 0\right] = \frac{H}{r};$$

$$\cos\theta(R,\alpha) = \frac{H_1}{r} = \frac{H}{r} = \cos\varphi(R,\alpha);$$

$$r(R,\alpha) = \left(H_1^2 + R_P^2 + R^2 - 2R_p R\cos\alpha\right)^{\frac{1}{2}} = \left(H^2 + R_P^2 + R^2 - 2R_p R\cos\alpha\right)^{\frac{1}{2}} \quad . \quad (2.3.3)$$

The general formula for calculating the thickness of the film takes the form (2.3.4):

$$h(R_p) = \int_{R1}^{R2}\int_0^{2\pi} \frac{\cos\varphi^2(R,\alpha)\;\; R\cdot\Pi(R)}{r^2(R,\alpha)\cos\gamma} d\alpha\, dR = \int_{R1}^{R2}\int_0^{2\pi} \frac{\left(\frac{H}{r}\right)^2 R\cdot\Pi(R)}{\left(\sqrt{H^2 + R_P^2 + R^2 - 2R_p R\cos\alpha}\right)^2\cos 0} d\alpha\, dR =$$

$$= \int_{R1}^{R2}\int_0^{2\pi} \frac{\left(\frac{H}{\sqrt{H^2 + R_P^2 + R^2 - 2R_p R\cos\alpha}}\right)^2 R\cdot\Pi(R)}{\left(\sqrt{H^2 + R_P^2 + R^2 - 2R_p R\cos\alpha}\right)^2\cdot 1} d\alpha\, dR = \int_{R1}^{R2}\int_0^{2\pi} \frac{H^2 R\cdot\Pi(R) d\alpha\, dR}{\left(\sqrt{H^2 + R_P^2 + R^2 - 2R_p R\cos\alpha}\right)^4} =$$

$$= \int_{R1}^{R2}\int_0^{2\pi} \frac{H^2 R\cdot\Pi(R)}{\left(H^2 + R_P^2 + R^2 - 2R_p R\cos\alpha\right)^2} d\alpha\, dR. \quad . \quad (2.3.4)$$

To simplify the calculation, the size of the system of evaporation will take some typical values. The diameter of the target can vary from 0.005 m to 5 m [3]. However, according to [4], MSS devices are most effective when the target has a relatively small diameter (50 - 75 mm).

The ratio $\frac{Rp}{Rav}$ varies in the range 0.2 … 1, the ratio $\frac{H}{Rav}$ varies in the range 0.6 … 2. Therefore, based on [4], we assume that: l = 36 mm; R_1 = 32 mm, R_{av} = 50 mm; R_2 = 68 mm; H = 20 ÷ 100 mm; R_p = 100 mm.

Dependence of the current density distribution along the radius of the target was obtained by two methods: using a target consisting of seven isolated rings, with each of them shot the proportion of the total current to the target, as well as by measuring the profile area sputtering target after a long period of MSS with constant parameters. The obtained data were approximated by a Langrange's polynom.

Langrange's polynom describes current density distribution along the radius of the target that is closest to the real. In this case, the general formula for calculating the thickness of film will take the form:

$$h(R_p) = \int_{R1}^{R2} \int_{0}^{2\pi} \frac{H^2 R \cdot P3(R)}{\left(H^2 + R_P^2 + R^2 - 2R_p R\cos\alpha\right)^2} d\alpha\, dR \quad . \qquad (2.3.5)$$

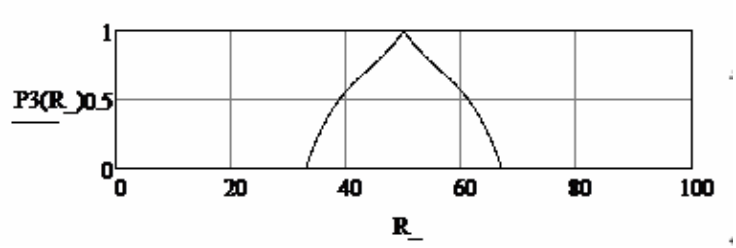

Fig.2.3.4. The current density distribution along the radius of the target, having the form of a polynomial of degree [4].

Now simulate the dependence for different values of the distance *H* from the substrate to the target.

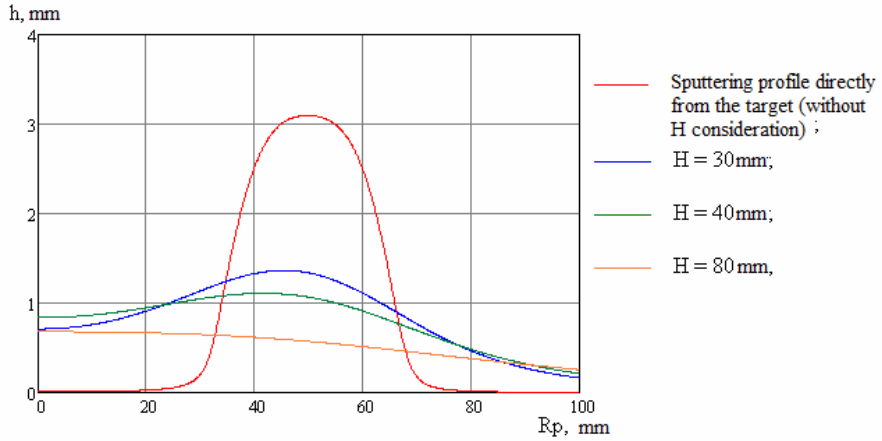

Fig. 2.3.5. The dependence of the thickness distribution of evaporated film on a substrate at different distances from the substrate to the target if the current distribution on the target plane is approximated by a polynomial of third power.

The film thickness in the approximation of the current density distribution third-degree polynomial describes the most real process.

In order to determine the geometrical parameters of film deposition was investigated in MSS uniform distribution of the film thickness (UDFT) on flat surfaces, depending on the angle of taper of the target and the ratio $\frac{H}{Rav}$.

Consider that the taper angle of the target is zero (flat disc) and let the distribution of current density along the radius of the target constant (P (R) = 1). We define a value at which the coating thickness on the maximum area will not change with an accuracy of ± 2%. To do this:

a) find the film thickness at the center of the substrate (i.e., when *Rp* = 0), as well as the ratio of film thickness at *Rp* ≠ 0 to the thickness of the film in the center of the substrate;

b) fix *Rav* and, by varying *N*, find a correlation of these variables, in which the ratio of thickness distributed over the substrate film to the film thickness at the center of the substrate will be close to 100%.

So, to find the beginning of the film thickness at the center of the substrate.

$$h_0\big|_{Rp=0} = \int_{R1}^{R2}\int_{0}^{2\pi} \frac{\cos\varphi^2(R,\alpha)\ \ R\cdot\Pi(R)}{r^2(R,\alpha)\cos\gamma} d\alpha\, dR = \int_{R1}^{R2}\int_{0}^{2\pi} \frac{H^2 R\cdot\Pi(R) d\alpha\, dR}{\left(\sqrt{H^2+R_P^2+R^2-2R_p R\cos\alpha}\right)^4} =$$

$$= \int_{R1}^{R2}\int_{0}^{2\pi} \frac{H^2 R\cdot\Pi(R)}{\left(H^2+0+R^2-2\cdot 0\cdot R\cos\alpha\right)^2} d\alpha\, dR = H^2 \int_{R1}^{R2} \frac{R\cdot\Pi(R)}{\left(H^2+R^2\right)^2} dR \quad . \quad (2.3.6)$$

The general formula for calculating the thickness of the film has the form:

$$h(R_p) = \int_{R1}^{R2}\int_{0}^{2\pi} \frac{H^2 R\cdot P2(R)}{\left(H^2+R_P^2+R^2-2R_p R\cos\alpha\right)^2} d\alpha\, dR \quad . \quad (2.3.7)$$

Thus, it is necessary to $\frac{h}{h_0} \to 100\%$.

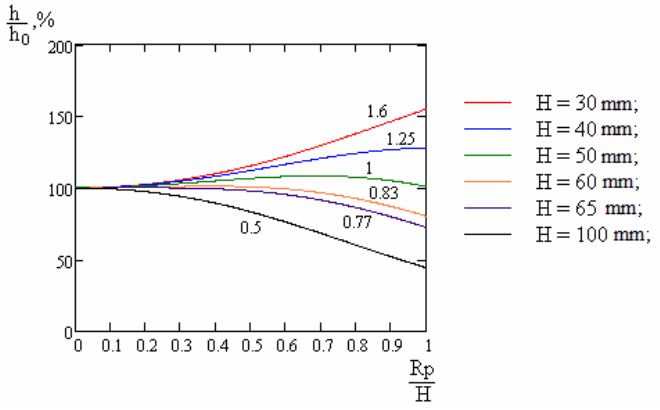

Fig. 2.3.6. The distribution of the film thickness for annular evaporator.

The numbers indicate the ratio of medium-range target *Rav* to the shortest distance to the evaporator *H.*

Fig. 2.3.6 shows that the largest UDFT average detected at *H* = 60 … 65 mm.

The calculation was fixed *Rav* = 50 mm. Thus

$$\frac{Rav}{H} = \frac{50}{65}...\frac{50}{60};$$
$$R_{av} = 0.77H...0.83H;$$
$$Rav \approx 0.8H; \quad H \approx 1.25R_{av}.$$

From this we can conclude that it is advisable to have a substrate at a distance $1.25R_{av}$ from the target to achieve the most uniform distribution of the thickness of the deposited film.

Now let's analyze the effect of taper angle on the profile of evaporated film with other equal parameters. We assume R_{av} = 50 mm and H = $1.25R_{av} \approx 60$ mm.

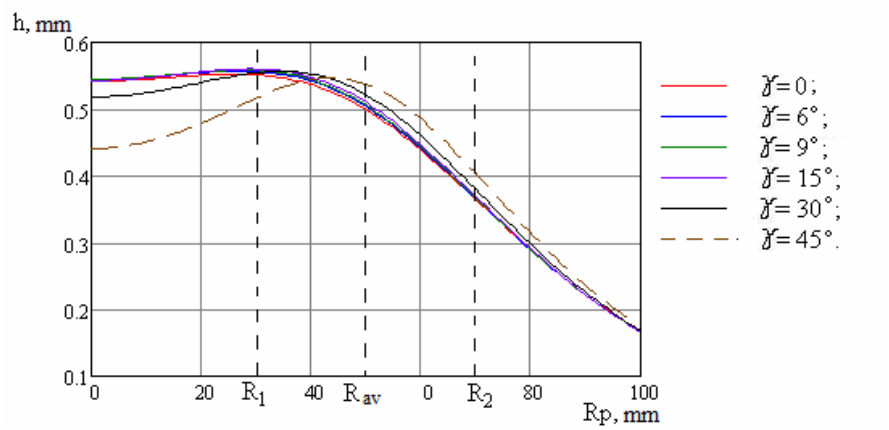

Fig. 2.3.7. The distribution of the film thickness for annular evaporator in the case of sputtering target in time, at different angles taper target.

Fig. 2.3.7. shows that achieving the highest distribution uniformity in thickness of the film occurs at small values of the cone angle *γ* (not more than 30 °).

With increasing *γ* in the areas of the substrate are directly above the cathode, there is a strong thickening of the evaporated film. In the center and edges of the substrate thickness, on the contrary, the area is strongly reduced (a redistribution of thickness). When γ> 30 idle mode is reached.

From this we can conclude that in order to maximize the area with high UDFT should not allow large values of γ, and adhere to the ratio $R_{av} \approx 0.8\ H$.

Based on the Danilin's model, a study of a profile of a sputtering target was conducted with a non-zero taper angle, and found the relation between the parameters of the MSS, in which the uniformity of distribution of the applied coating is the greatest.

It was found that the greatest uniformity of distribution of the film thickness is achieved with an average radius of the target $R_{av} \approx 0.8H$ (H is the shortest distance between the substrate and the target) and at small angles of taper ($\gamma < 30$ °).

The efficiency of the magnetron sputtering system depends on the correct choice of operating parameters. The stability of these parameters determines the constancy of the speed of deposition and reproducibility of the properties of the films.

3. Analysis of the processes occurring during the formation of oxide films by magnetron sputtering

The formation of HTS films by magnetron sputtering can be divided into the following dynamic phase [15]:

- Creation of the flow of charged and accelerated particles that bombard the target;
- Sputtering target under the influence of the accelerated flow of energetic particles;
- Transfer of sputtered atoms and atomic groups, knocked out of the target to the substrate;
- Adsorption, condensation, formation of the film [16].

These process stages are implemented in certain areas of space "target-substrate", marked in Fig. 3.1. It shows a typical distribution of the potential U (x) in cathode sputtering dc. In the simulation used a straightforward approximation, in which the total potential drop $U(x)$ is in the area of the cathode dark space (CDS).

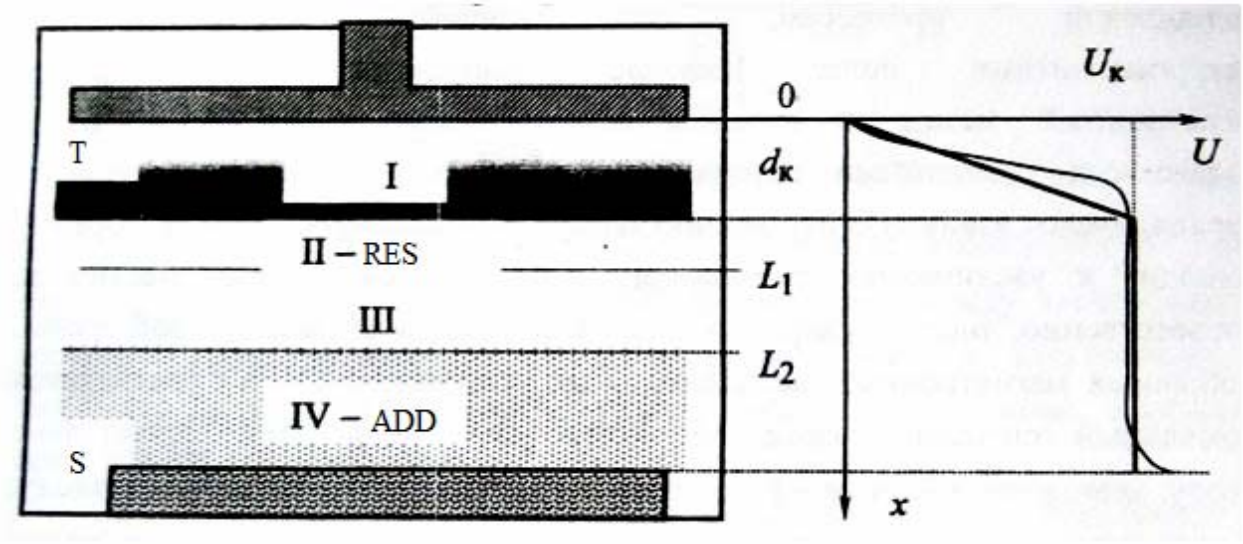

Fig. 3. 1. Model representation of the process in certain areas of space "target-substrate", where the T is target; S is substrate; I is cathode dark space (CDS); II is region of elastic scattering (RES); III is region of thermalization (RT); IV is area of the diffusion distribution of sputtered atoms (ADD). [16]

The main tasks of modeling of film deposition is to determine the relative position of the substrate and the target and estimate the rate of growth of the film v_p.

A brief review of these sequential stages is given in order to assess the possibility of their analytical modeling.

3.1 Creation of the flow of charged and accelerated particles that bombard the target

Creating a flow of accelerated particles that bombard the target is in an abnormal glow discharge in inhomogeneous crossed electric and magnetic fields that actually can't give an exact analytical description of phenomena occurring. At the same time, it is possible to evaluate the energy spectrum of sputtered particles, the density of spray flow and the thickness of the near-cathode layer.

For a glow discharge gas existence processes occur in its cathode region. It is a cathode dark space (CDS). The positive discharge column and anode space perform the passive role of a conductor with high electrical conductivity, which connects the cathode to the anode region.

In the glow discharge electrons emitted from the cathode have small initial velocities, determined by their work function of the cathode. Therefore, the collisions of the atoms in a thin layer of gas near the cathode show purely elastic nature.

As we move downside potential from the cathode in a strong electric field of the cathode, electrons gain energy and speed of their movement increase. The motion of electrons occurs in the gas and the average velocity of directed motion is achieved.

At some distance from the cathode electron energy is taken only to ionize the atoms. This leads to the formation of charged particles. Large velocities of directed motion of electrons and small velocities of directed motion of ions in the time of their generation promote formation in the CDS excess space charge. Spatial dependence of the potential distribution reaches a maximum here, and the electric field intensity drops almost to zero. With this boundary region cathode potential drop is approximately equal to the upper limit of the CDS.

The emitted electrons from the cathode surface, breaking the CDS and the positive column discharge plasma, are practically without collisions bombard the anode and the substrate with energies of voltage level, i.e. the order of 1 keV [23]. This can lead to significant heating of the substrate to 400 ...600 ° C and it prevents the sedimentation by cathode sputtering of low-melting compounds.

The function of the energy distribution of ions and neutrals bombarding the target in glow discharge plasma can set based on a modified formula Keller and Simmons characterizing cathode sputtering. The formula below (3.1) can also be used to consider the process of magnetron sputtering in a glow discharge in view of the potential distribution function $\varphi(x)$ in the CDS:

$$I(d_k, E) = \frac{d_k}{\lambda_i e U_k} * \exp\left(-\frac{d_k U}{\lambda_i * U_k}\right) + \exp\left(-\frac{d_k}{\lambda_i}\right) * \delta(eU - eU_k)$$
$$A(d_k, E) = \left[\frac{d_k}{\lambda_i e U_k} \exp\left(-\frac{d_k U}{\lambda_i * U_k}\right)\right]\left[1 + \frac{d_k}{\lambda_i}\left(1 - \frac{U}{U_k}\right)\right] \quad , \qquad (3.1)$$

where d_k is the thickness of the near-cathode layer; e is unit charge; λ_i is mean free path of ions; $E_k = eU_k$ is energy corresponding to the voltage applied to the target; $\delta(E-E_k)$ is Dirac delta function. To assess the value of d_k, the model of the near-cathode layer can be used in the case of magnetron sputtering [4]:

$$d = \left(\frac{\lambda_e}{\omega\tau}\right) \ln\frac{1}{\gamma} \quad , \qquad (3.2)$$

where λ_e is mean free path of electrons on the ionization, ω is speed of the particle, τ is the mean free time, γ is coefficient of electron-ion emission. Equation (3.2) includes options nondescript and therefore for the purpose of modeling can be used more than a simple expression [5]:

$$d = \left(\frac{2m_e U_c}{e}\right)^{\frac{1}{2}} * \frac{1}{B_c}, \qquad (3.3)$$

where B_c is the magnetic field in the CDS; m_e, e are electron mass and charge, respectively.

The experimental results of the current-voltage characteristics and energy spectra of ions bombarding the cathode for high current abnormal gas discharge [24] show that the majority of ions enters the CDS from the positive column plasma.

This suggests that the flux of ions moving in the direction of the border "plasma-CDS" to the cathode target, in any section in the CDS at this distance can be considered constant.

Spray flux density is calculated using the formula (3.4), in which the mean free path of an ion is equal to the length of the path of an atom of the working gas: $\lambda_i = \frac{4kT}{p\delta_a^2}$.

$$Q_i = \frac{j}{e(1+\gamma)}; \qquad Q_\Sigma = Q_i\left(1 + \frac{d_k}{\lambda_i}\right), \qquad (3.4)$$

where Q_i is the flux density of ions; Q_Σ is the total flux of atoms and ions arriving at the target surface; *j* is particle flux density; *e* is electron charge; γ is coefficient of electron-ion emission is usually assumed to be 0,1 ... 0,3. To determine the current density it is necessary to take into account the uneven sputtering of the target, i.e. current density will be equal to the quotient of the value of the discharge current on the size of the area of erosion.

The calculations conventionally assumed that the effectiveness of spraying concrete targets for charged and neutral particles of the same nature as the same [6]. Depending on the parameters of the magnetron discharge and, basically, on the value of the parameter d/λ_i flux density of ions and neutrals can vary and, accordingly, change their contribution to the etching rate of the target.

3.2. Sputtering target under the influence of the accelerated flow of energetic particles

The process of physical sputtering is the result of the combined flow of the accelerated particles with the target surface. The main characteristic of this process is the sputtering coefficient- *Y*. There are partial *Yj*, i.e. coefficient characterizing the output of atoms (particles) of sort *j* of the target of complex composition and effective integral factor for the composition of the target. Atomized flow from the target is characterized by the partial and the integral density of atoms Γ_j and Γ_Σ, respectively, as well as by the energy distribution. *Y* is determined as follows:

$$Y = \int_{E_0}^{E_c} Y(E)[A(d,E) + B(d,E)]dE \quad , \tag{3.5}$$

where E_o is the threshold energy for sputtering, coefficients *A* and *B* can be found from (3.1). To assess the value of E_o can use a formula based on the theory of Sigmund [7]:

$$E_o = \frac{(M_1 + M_2)^2}{M_1 M_2} E_b \quad , \tag{3.6}$$

where E_b is binding energy component in the lattice, eV; M_1 and M_2 are the mass of the atoms of the incident particle and target, respectively.

The most simplified formula in the low-energy range of the energy of the ion beam is a Shteinbruhell expression [8]. This gives a fairly good agreement with experimental values of the sputtering yield. In this formula there are no given values of energy, no residual inhibition of expressions section or mass of the ion and target atom. The formula substituted only the values of the atomic number of the ion, the target material and the coefficients *A* and β:

$$Y(E) = \frac{Az_2}{E_{con}(z_1^{2/3} + z_2^{2/3})^{3/4}} \left(\frac{z_1}{z_1 + z_2}\right)^{\beta} E_1^{1/2}, \quad (3.7)$$

where z_1 and z_2 are the serial numbers of atoms of the incident particle and target, respectively; E_{con} is binding energy, eV; E_1 is energy sputtered particles in the spectrum, keV; A and β are approximation coefficients, coefficients A = 5.2 and β = 0.67 which correspond to ions of argon and the average atomic number of the target. When changing the sputtering conditions and the preservation of low energy ions, the values A and β change slightly.

The criterion of applicability of the formulas of the sputtering is experimental results. The coefficient of dispersion is determined by the mass change of the target before and after exposure to monoenergetic ion beams in an extremely clean process environment. Strong influence on the experimental values of the coefficients shows the nature of the target and the state of its surface. The more persistent is the metal oxide, the greater the difference between the experimental and calculated values of the sputtering.

Atomized flow is partial and integral density Γ_j and Γ_Σ respectively. Partial stream of particles emitted from the target can be defined as follows:

$$\Gamma_j = \nu_j Q_i \left(1 + \frac{d_k}{\lambda_i}\right) R, \quad (3.8)$$

where Γ_j is stoichiometric proportion of the component of the target. The total flux of particles is represented as the sum of the partial flows.

3.3. Transfer of sputtered atoms and atomic groups, knocked out of the target to the substrate

Analysis of the transfer of atoms from the target to the substrate. The process of transfer of atoms from the target to the substrate includes the following stages:

1 - Explore directed to the substrate particle flow;

2 - Scattering of fast sputtered particles on the atoms of gas (regions I and II, see Fig.3.1), provided that the energy of sputtered particles exceeds the average thermal energy of gas atoms;

3 - Thermalization (region III), i.e. the process of aligning the energy of sputtered particles with the thermal energy of the gas medium. In terms of the scattering of multicomponent particle flux thermalization occurs for each component is different due to differences in mass and energy with which the particles leave the target;

4 - Diffusion scattering of sputtered particles (VI).

Note that in the space of a target-substrate is presented ionic component of the gaseous medium with different charges and the fast electrons. These electrons are also involved in the transfer process in a magnetic sputtering in accordance with the potential distribution in the space of a target-substrate.

To analyze the transport process of sputtered flux can be used various methods based on a single theoretical approach can be used [9]. In the region I and II are considered the collisional processes of accelerated particles in a gaseous environment of the statistical-based models of hard spheres. Here we consider only elastic collisions, which resulted in no change in the internal and kinetic energy of the colliding particles. In one act of elastic collisions of sputtered atoms (M_1) is scattered at an angle β, in the laboratory system of coordinates (LSC). From the theory of elastic collisions is known [9] that the scattering angle of the incident particle is more convenient to determine the center of mass (CM), but the LSC is more convenient for the analysis of elastic scattering of particles. The scattering angle in the CM - θ is associated with the angle β following equation:

$$tg\beta = \frac{sin\theta}{M_1/M_2 + cos\theta}, \qquad (3.9)$$

from which it follows that $M_1 > M_2$, a first approximation we can assume that $\beta \approx arcsin {}^{M_2}/_{M_1}$. This means that for conditions when the mass of the scattering atom greatly exceeds the mass of the scattering center, the accelerated flow of particles scattered in the direction of a narrow cone of forward. In elastic scattering components we have chosen systems, the condition $M_1 > M_2$, and thus we can assume that the change in flux density of fast-atom elastic scattering on the atoms of argon (oxygen) doesn't take place.

The average number of collisions N sputtered to a state of thermalization can be calculated by the following formula:

$$N_j = \frac{\lg ({}^{E_a}/_{E_{02}})}{\lg (1-\kappa)}, \quad (3.10)$$

where E_a is average energy of the atom gas medium, determined by the temperature of the working gas; E_{02} is average energy of atoms ejected from the target surface; κ is average share of energy transfer, calculated by the formula (3.11).

$$\kappa - 4\frac{m_i m}{(m_i+m)^2}, \quad (3.11)$$

where m and m_i are mass of the electron and ion, respectively. Since $m_i >> m$, then $\kappa = 4\ m/m_i$. An electron must undergo many collisions to transfer excess energy atoms. The energy exchange between electrons is parallel with the acquisition of energy by electrons from the external source of power and caring energy from the plasma by radiation and heat. After 6 - 12 collisions virtually all spray flow thermalized, knocked out of the target atoms are in the regime of diffusive propagation in the direction of the substrate.

The collision of sputtered atoms in the plasma gas discharge will be considered only with the gas atoms, since the concentration of ions and electrons is much smaller than the concentration of atoms (degree of ionization is less than 10^{-3}). Calculated mean free path of sputtered atoms in the formula is

$$\lambda_j = \frac{4kT}{\pi(\delta_1+\delta_2)^2 P\left(1+{}^{M_2}/_{M_1}\right)^{1/2}}, \quad (3.12)$$

where δ_1, δ_2 are diameter of the gas and sputtered atoms, respectively, the average length of the directed motion of atoms to a state of thermalization can determine:

$$L_j - \lambda_j N_j. \quad (3.13)$$

The adopted averaging help to determine the coordinates of the area III, in which the thermalization of sputtered particles take place, as well as set the technological factor d-distance "target-substrate". In order to suppress the effects resputtering of the film and the diffusion care component of the region of the substrate to chamber wall deposition distance "target-substrate" to be considered with technological relations $d \sim 1,5\ L_k$.

To analyze the process of moving atoms in magnetron sputtering often is used standard mathematical procedure based on the Monte Carlo test particle [22]. The calculation of the Monte Carlo method of spatial and energy characteristics of the flow of sputtered atoms in a cylindrical discharge chamber is made in the pair collision approximation. Modeling scattering involves identifying a series of possible outcomes of random events. The trajectory of a "model" of the particle will not, of course, coincide with the trajectory of sputtered atoms in a real process, but the "collective property", for example, the average particle displacement in one collision is sufficiently close to the real.

The practical importance is the design function of changes in the density of the total flux Γ_Σ sputtered particles in the space of "target-substrate" for the various positions along the radius of the substrate.

After attaining the state of thermalization, the sputtered atoms are distributed in accordance with the laws. Diffusion for $d > L_k$ grows in accordance with a stream of atoms that move away from the substrate, which leads to a decrease in the rate of deposition. As a result, the analytical approximation of the relative flux density of sputtered atoms was obtained by following expression:

$$\Gamma_{jd} = \Gamma_{j0} \frac{\chi\lambda_j}{\chi\lambda_j + \beta(\sqrt{x} - \sqrt{L_j})^2}, \quad (3.14)$$

where χ and β are fitting coefficients. These are χ = 1,052 and β = 0.975 and depend only weakly on pressure and temperature of environment for the chosen parameters.

3.4. Adsorption, condensation, formation of the film

Deposition of sputtered flux and the growth of the film. For the transport process of sputtered atoms on the valuation level enough to take the values of adjustable parameters equal to unity. Thus, by setting the discharge current density, we can determine the density of the partial flow of sprayed at the coordinate *x* or *d*, in the light scattering function of atomized flow (3.5):

$$\Gamma_{jx} = \frac{\upsilon_j jR}{e(1+\gamma)}\left(1+\frac{d}{\lambda_i}\right)f(x,P,T) = \frac{\upsilon_j jR}{e(1+\gamma)}\left(1+\frac{d}{\lambda_i}\right)\frac{x\lambda_j}{[x\lambda_j+\beta(\sqrt{x}-\sqrt{L_j})^2]}. \qquad (3.15)$$

To calculate the deposition rate necessary to determine the capture coefficient of condensation components-S_j *(T).* In the initial approximation, it can be the same for all components of the film-*S (T).* Using (3.13) and (3.14), we express the rate of deposition as follows:

$$\upsilon_o = \frac{S(T)\mu_\Sigma j}{gN_A}\sum_k\left[\frac{\upsilon_j R}{e(1+\gamma)}\frac{\lambda_k}{[\lambda_k+(\sqrt{d}-\sqrt{L_j})^2]}\right], \qquad (3.16)$$

where $\mu_\Sigma=\Sigma\upsilon_j\mu_j$ is the total mass number.

As a result, model review and analyze the experimental transport data of sputtered atoms from the target to the substrate with the expression (3.14). This is used in approximate calculations the deposition rate of films during ion-plasma sputtering of composite targets. The formula contains the sputtering coefficient *R*, which is 70...75% of the value corresponding to a monoenergetic ion beam sputtering with an energy equal to the U_k.

4. Discussion the results of modeling

It is assumed that the thermalized sputtered atoms lose its direction and diffuse through working gas. If we restrict the consideration of one-dimensional problem, then eventually diffusing atoms are deposited either on target or on the anode. Based on this assumption, as well as from the first Fick's law, we obtain the following expression for the flux density of sputtered atoms that have reached the anode:

$$\Gamma_a(x) = \frac{L_k * arctg(D/L_k)}{D} * \Gamma_a(0) \quad (4.1)$$

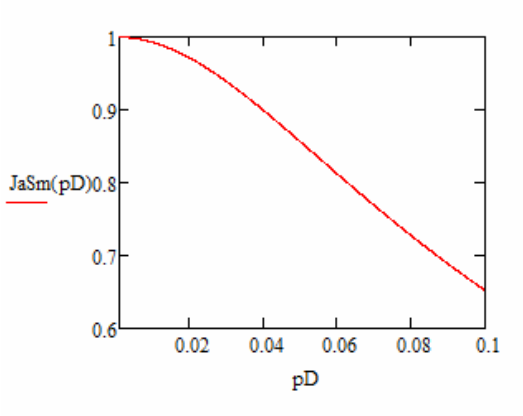

Fig. 4.1 Dependence of the efficiency of the transport of sputtered atoms Sm to the anode through the atmosphere of Ar.

The efficiency of delivery of the sprayed material to the anode can be characterized by the size ratio $\Gamma_a(x)/\Gamma_a(0)$. In Fig.4.1 is shown calculation of the relationship of $\Gamma_a(x)/\Gamma_a(0)$ produced for the case of sputtering of samarium in argon. As can be seen from the figure at not too low pressures (in this case *pD* ≥ $5*10^{-2}$ Pa*m) effective transport of sputtered atoms is inversely proportional to the value of the *pD* product. This is consistent with known empirical regularities.

The process of diffusion of flight of sputtered atoms in the thermalized flow can be estimated using the expression (4.2):

$$\frac{\Gamma_{\Sigma,x}}{\Gamma_{\Sigma,0}} = \frac{\chi * \chi_1 {}^{T}/_{p}}{\chi * \chi_1 * \frac{T}{p} + \beta * (\sqrt{x} - \sqrt{\chi_1 * N * {}^{T}/_{p}})^2}, \quad (4.2)$$

where N is the average number of collisions N sputtered to a state of thermalization, $\chi = \beta = 1$ are fitting coefficients, $\chi_1 = 1.21*10^{-5}$ m*Pa/K. If we take into account that T = 500K, p = 11 Pa and x = 10 mm and making the substitution, we obtain the dependence of the total flux of the distance target-substrate. Comparing it with the experimental dependence, one can observe that the model we have used can quite adequately describe the transition process of sputtered atoms and to determine density of sputtered flow in any point of target-substrate area, with different basic technological factors (*p,d,T*).

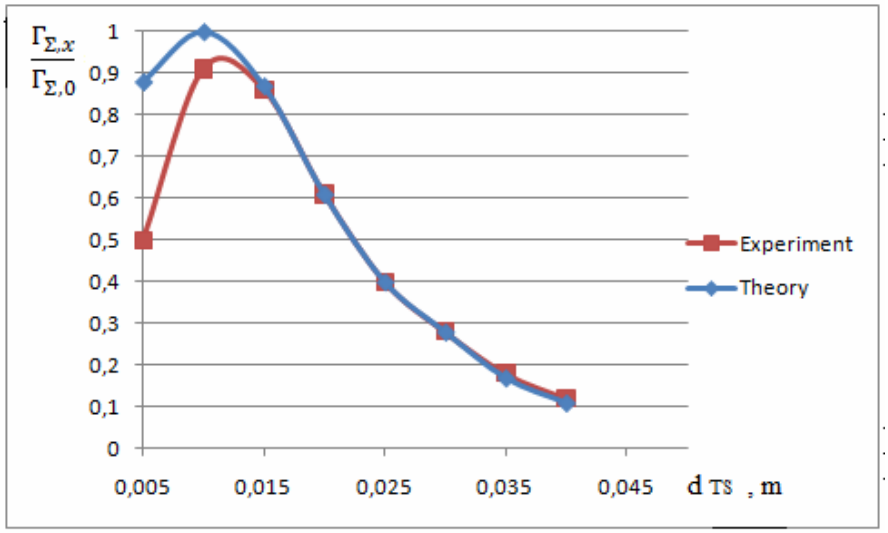

Fig.4.2. The dependence of the total flux on the target-substrate distance.

As it is shown at the Fig. 4.2 the proposed model has good results in comparison with the experimental results. Both curves are almost identical at the average values of distance “target- substrate”, so we can make a conclusion that the model, presented in this work, shows good results, which are supported by experimental research.

With the help of the model we can calculate velocities with changing discharge current density and find their dependence.

Table 2. Velocity dependence velocity on discharge current density for Fe-based superconductor: $SmFeAsO_{7-\delta}$.

Parameter/Values									
j, mA/cm^2	5	10	15	20	25	30	35	40	45
V, pm/s	6.268	12.54	18.8	25.07	31.34	37.61	43.8	50.14	56.41

Table 3. Velocity dependence on discharge current density for YBCO superconductor.

Parameter/Values									
j, mA/cm^2	5	10	15	20	25	30	35	40	45
V, pm/s	9.077	18.15	27.23	36.31	45.39	54.46	63.54	72.62	81.69

According to these tables, one can see that velocity increases linearly with increasing current density. This effect will be up to high values of current densities, such as 65 mA/cm^2 for cooper, when sputtering process evaporation begins to play significant part in the sputtered process.

Now let's compare these two dependences and describe the reason of their difference.

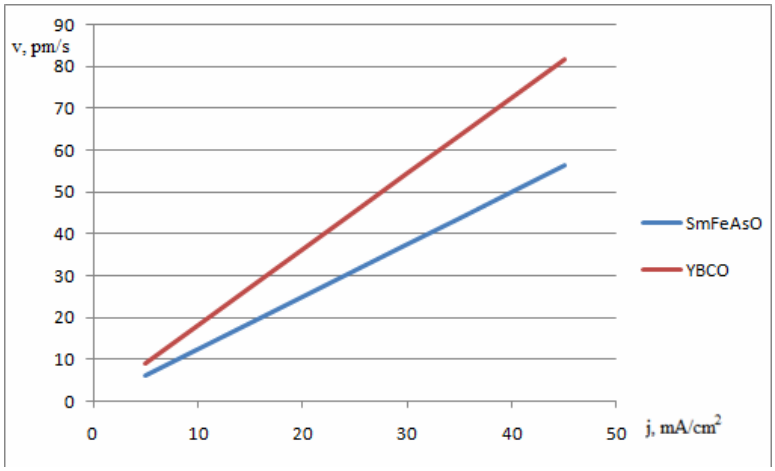

Fig. 4.3.Velocity dependence on discharge current density for $SmFeAsO_{7-\delta}$ and YBCO.

If we compare these two dependences it is obvious that YBCO has bigger values of velocities than Fe-based. It is understandable while taking into account the fact that Fe-based material has components which are complex for sputtering. They have ionization energy more than the components of YBCO.

Conclusion

Nowadays the interest for the superconductors grows again because of their relevance in modern techniques and of opening new types of HTS. Although these new materials are not well discussed and explored, they present a great interest for scientists all over the world.

The aim of this work was to explain the main processes which take part at the magnetron sputtering and to calculate values, describing them. Analysis of the stages of technological process of formation of oxide films during magnetron sputtering revealed that among the four conventional stages, the last stage of condensation of sputtered particles and the "*in-situ*" formation of the structure is the most important. Using the characteristics of the MSS we may evaluate the density and composition of the sputtered flux components.

In this work was also briefly discussed distribution of coating thickness in planar magnetron sputtering system to understand the principles of location substrate versus target. Calculation shows that in order to maximize the area with high UDFT should not allow large values of γ, and adhere to the ratio $R_{av} \approx 0.8H$.

Two types of superconductors were analyzed: well-known YBCO cuprate and new Fe-based superconductor $SmFeAsO_{7-\delta}$. Simulations were made for both of them and in the end we compare theoretical results with the experimental ones for YBCO.

The difference between these results was acceptable: theoretical results were almost the same like the experimental ones at the most important part of the dependence. So the model, represented at this work, adequately reflects the main physical processes and can be used in future for modeling basic parameters of the processes in the magnetron sputtered system.

The result of this work were published in annual conference of finnish physical society [24].

References

1. Thomsen C., Cardona M. – in “Physical Properties of High-Temperature Superconductors”, ed. By D. M.Ginsberg (World Scientific, Singapore, 1989) p. 409.

2. Hideo Hosono - Iron Pnictide Superconductors: Discovery and Current status. // Material Matters, 2009, vol. 4, no.2, pp.34.

3. Барченко В.Т., Быстров Ю.А.,. Колгин Е.А. «Ионно-плазменные технологии в электронном производстве»: Санкт-Петербург, «Энергоатомиздат», 2001.

4. Данилин Б.С. «Применение низкотемпературной плазмы для нанесения тонких пленок»: Москва, «Энергоатомиздат», 1989.

5. Kamihara Y., Watanabe T., Hirano M. and Hosono H.: J. Am. Chem. Soc. 130(2008) 3296.

6. Chen G. F., Li Z., Li G., Zhou J., Wu D., Dong J., Hu W. Z., Zheng P., Chen Z. J., Luo J. L., Wan N. L.: Superconducting properties of Fe-based layered superconductor $LaO_{0.9}F_{0.1}$- _FeAs: arXiv: 0803.0128.(2008).

7. Ishida Kenji, Nakai Yusuke, Hosono Hideo To what extend iron-pnictide new superconductors have been clarified: a progress report: arXiv: 0906.2045v1.(2008).

8. Някшев К. Ф. Разработка и исследования процесса формирования сверхпроводниковых пленочных структур для применения в СВЧ электронике. //Диссертация на соискание ученой степени кандидата технических наук.- Л.: ЛЭТИ.- 1994, -219 с.

9. Masterov D. V., Pavlov S. A., Parafin A. E. and Drozdov Yu. N. Thin films of YBaCuO high-temperature superconductor growth in a simplified magnetron sputtererring system and their microwave application. //Technical Physics, 2007, vol. 52, no. 10, pp. 1351-1355.

10. Hai- Hu Wen - Developments and perspectives of iron-based high-temperature superconductors. // Advanced Materials, 2008, vol. 20, pp. 3764-3769.

11. Zhao J., Chern C. S., Li Y. Q., Noh D. W., Gallois B. – In-situ growth of YBCO high-Tc superconducting films by plasma- enhanced metal organic chemical vapor deposition.// J. Cryst. Growth. 1991, 107, 699-704.

12. Акопьян В., Паринов И., Stephen Chang. Сверхпроводимость: методы получения высокотемпературных сверхпроводников. // Научно-культурологический журнал. 2010, 2.

13. Вольпяс В. А., Гольман Е. К., Цукерман М. А. Исследование процессов термализации и диффузии потоков распыленных атомов в газах. //Журнал технической физики, 1996, 4, стр. 16-23.

14. Вольпяс В. А., Козырев А. Б., Афанасьев В. П. Моделирование процессов распыления и переноса в ионно-плазменной технологии. СПб.: ООО «Техномедиа» / Изд-во «Элмор», 2007.154 с.

15. Карманенко С. Ф., Бобыль Ф. В., Семенов А. А. Анализ технологических режимов процесса ионно-плазменного распыления: Методические указания к практическим занятиям по дисциплине «Технология материалов и изделий электронной техники». СПб.: Изд-во СПбГЭТУ «ЛЭТИ», 2004. 32 с.

16. Зайцев А. Г. Исследование процесса магнетронного распыления с целью получения сверхпроводниковых покрытий. // Диссертация на соискание ученой степени кандидата технических наук. Санкт- Петербург, 1991.

17. Данилин Б. С. Методы нанесения пленок высокотемпературных сверхпроводников // Итоги науки и техники. Сер. Электроника. М.: ВИНИТИ, 1990, т.26, с. 133-170.

18. Abril I., GrasßMarti A., Valles Abarca J. A. The contribution of fast neutrals to cathode erosion in glow discharge. // J.Phys.D.:Appl.Phys. , 1984, v.17, n.9, 1841-1849.

19. Sigmund P. Theory of sputtering. Sputtering yield of amorphous and polycrystalline targets. // Phys. Rev., 1969, v.184, n.2, p. 383-416.

20. Steinbruchel C. A simple formula for Low-Energy Sputtering Yields // Appl. Phys. A. 1985. A36. P.37-42.

21. Моделирование процесса переноса частиц при ионно-плазменном распылении.: Методические указания к курсу лекций. Вольпяс В. А., Гольман Е. К., Зайцев А. Г., Розин С. Е. – Препринт СПбГЭТУ, - СПб, 1991, - 28 с.

22. Ball D. J. Plasma Diagnostics and Energy Transport of a dc Discharge Used for Sputtering // J. Appl. Phys. 1972. Vol. 43, № 7. p. 3047- 3057.

23. Neu H. Theorie der Strom - Spannugs - Charakteristik der Stationären Glimmentladung //Z. Phys. 1959. Bd. 155, № 1. S. 77-100.

24. N. Nikitina, V. Barchenko, E. Lahderanta Modeling of processes in the magnetron sputtering system with high current densities, Proceedings of the XLIV annual conference of finnish physical society March 11-13, 2010, Jyvaskyla, Finland

25. Imperial College London, 2006. Yttrium Barium Copper Oxide - YBCO [Online] (Updated 25 Aug 2006). Available at: http://www.ch.ic.ac.uk/rzepa/mim/century/html/ybco_text.htm [Accessed 19 May 2010]

26. Hiroki Takahashi. Rapid Development of Study in Iron-based New Superconductors, June 10, 2008: jpsj.ipap.jp/news/jpsj-nc_35.html

Appendix 1.

Algorithm for the iron-based superconductor $SmFeAsO_{7-\delta}$

1. Specify basic parameters of the components of the superconducting material

Initial physical quantities for calculating the parameters of film deposition

Sm	Fe	As	O	Ar	
$\nu kSm := 0.25$	$\nu kFe := 0.25$	$\nu kAs := 0.25$	$\nu kO := 0.2225$		gram atomic stoichiometric ratio
$\delta kSm := 1.928$	$\delta kFe := 1.28$	$\delta kAs := 0.92$	$\delta kO := 2.64$	$\delta aAr := 3.76$	atom's diameter, A
$EcbSm := 5.6$	$EcbFe := 4.3$	$EcbAs := 9.81$	$EcbO := 13.61$		cation's connection energy, eV/at
$zSm := 62$	$zFe := 26$	$zAs := 33$	$zO := 8$	$zAr := 18$	serial number
$mSm := 150.6$	$mFe := 55.847$	$mAs := 74.921$		$mAr := 39.949$	atomic weight, gr/mol

2. Specify basic parameters of the MSS

$Uk := 0.5$ kV — cathode voltage

$j := 5$ $\frac{mA}{cm^2}$ — discharge current density

$p := 10$ Pa — pressure of working gas

Modeling basic processes in the "target-substrate" region

1. Creation of the flow of charged and accelerated particles that bombard the target.

The thickness of the near-cathode space:

$$dk := \left(2 \cdot 10^{-2} \cdot \frac{Uk^3}{j^2 \cdot p}\right)^{\frac{1}{5}}$$

$dk = 0.1$ cm

$dk := 0.001$ m

Determining density of the ion flux Qi

$el := 1.67 \cdot 10^{-19}$ C — electron charge

$\gamma := 0.1$ — coefficient of electron-ion emission

$$Qi := \frac{j}{el \cdot (1 + \gamma)}$$

$Qi = 2.722 \times 10^{19}$ $cm^{-2} \cdot c^{-1}$

Determining total flux of atoms and ions Qsum

$k := 1.38 \cdot 10^{-23}$ $\frac{J}{K}$ Bolzman coefficient

$Temp := 873 \quad K$ temperature

$$\lambda i := \frac{4 \cdot k \cdot Temp}{p \cdot \left(\delta aAr \cdot 10^{-10}\right)^2}$$

$\lambda i := 23.4268910^{-3}$ m

$$Qsum := Qi \cdot \left(1 + \frac{dk}{\lambda i}\right)$$

$Qsum = 2.838 \times 10^{19}$ $cm^{-2} \cdot m^{-1}$

2. Sputtering target under the influence of the accelerated flow of energetic particles

Calculating sputtering glow discharge

$Ek := el \cdot Uk$

$Ek := 0.5$ eV energy corresponding to the voltage applied to the target

for Sm

$$\chi Sm := \frac{mAr \cdot mSm}{(mAr + mSm)^2} \qquad EporSm := \frac{EcbSm}{2 \cdot \chi Sm}$$

$EporSm = 16.898$ eV

for Fe

$$\chi Fe := \frac{mAr \cdot mFe}{(mAr + mFe)^2}$$

$$EporFe := \frac{EcbFe}{2 \cdot \chi Fe}$$

$EporFe = 8.844$ eV

for As

$$\chi As := \frac{mAr \cdot mAs}{(mAr + mAs)^2}$$

$$EporAs := \frac{EcbAs}{2 \cdot \chi As}$$

$EporAs = 21.624$ eV

Determining integral energy distribution of ions in the target plane

$$c := 1 + 0.5\left(\gamma^{\frac{-1}{2}} - 1\right)$$

$$h(x) := 1 - \frac{x}{c} - \left(1 - c^{-1}\right)\cdot x^2$$

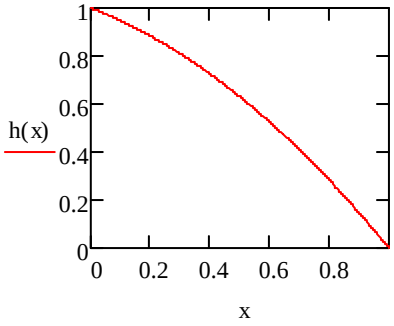

Calculating integrated effective sputtering coefficient and partial density of atomized flux

for Sm

$$YSm(E) := \frac{5.2\cdot zSm}{EcbSm\cdot\left(zAr^{\frac{2}{3}} + zSm^{\frac{2}{3}}\right)^{\frac{3}{4}}}\cdot\left(\frac{zAr}{zAr + zSm}\right)^{0.67}\cdot\left(\frac{E}{1.4}\right)^{\frac{1}{2}}$$

EporSm = 16.898 eV

$$hk := \left(\frac{1.67\cdot 10^{-19}\cdot\lambda i}{mAr\cdot 1.67\cdot 10^{-27}}\right)^{\frac{2}{5}}\cdot\left[4\cdot 8.85\cdot 10^{-12}(1+\gamma)\right]^{\frac{2}{5}}\cdot\frac{\left(Uk\cdot 10^{3}\right)^{\frac{3}{5}}}{\left(j\cdot 10^{1}\right)^{\frac{2}{5}}\cdot p^{\frac{1}{5}}}$$

hk = 0.03

elUk := 1

$$eU := 0, 10^{-2}..1$$

$$I(E) := \frac{1.2}{23.4268}\cdot\exp\left(\frac{-10\cdot E}{23.4268\,elUk}\right) + \exp\left(\frac{-12}{23.4268}\right)\delta(E - 1)$$

$$I\_1(E) := \frac{30}{23.4268}\cdot\exp\left(\frac{-30\cdot E}{23.4268\,elUk}\right) + 0$$

$$I\_2(E) := 0 + \exp\left(\frac{-30}{23.4268}\right)\cdot\delta(eU - 1)$$

$$A(E) := \left(\frac{30}{23.4268}\exp\left(\frac{-30E}{23.4268\,elUk}\right)\right)\cdot\left[1 + \frac{30}{23.4268}\cdot\left(1 - \frac{E}{elUk}\right)\right]$$

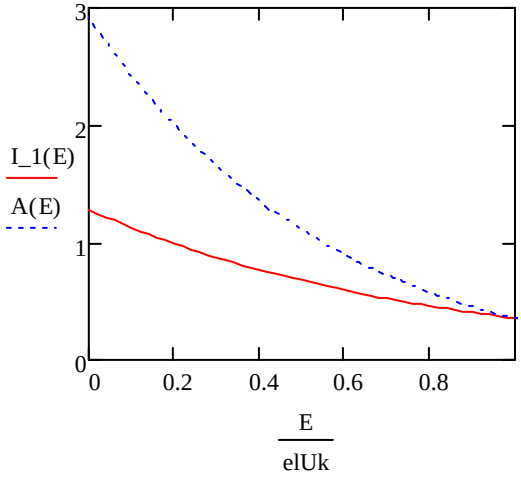

$$RSm := \int_{Ek}^{EporSm} YSm(E)\cdot(I(E) + A(E))\,d(E)$$

$$RSm1 := \int_{Ek}^{EporSm} YSm(E)\cdot(I\_1(E) + A(E))\,d(E) \qquad RSm1 = 1.359$$

$$RSm2 := \begin{cases} \exp\left(\frac{-30}{23.4268}\right)\cdot YSm(0.5) & \text{if } Ek \le 0.5 \le EporSm \\ 0 & \text{otherwise} \end{cases} \qquad RSm2 = 0.34$$

$$RSm := RSm1 + RSm2$$

$$\Gamma kSm := \nu kSm\cdot Qi\cdot\left(1 + \frac{dk}{\lambda i}\right)\cdot RSm$$

$$\Gamma kSm = 1.205\times 10^{19} \quad cm^{-2}\cdot s^{-1}$$

for Fe

$$YFe(E) := \frac{5.2\cdot zFe}{EcbFe\cdot\left(zAr^{\frac{2}{3}} + zFe^{\frac{2}{3}}\right)^{\frac{3}{4}}}\cdot\left(\frac{zAr}{zAr + zFe}\right)^{0.67}\cdot\left(\frac{E}{1.4}\right)^{\frac{1}{2}}$$

$$RFe := \int_{Ek}^{EporFe} YFe(E)\cdot(I(E) + A(E))\,d(E)$$

$$RFe1 := \int_{Ek}^{EporFe} YFe(E)\cdot(I\_1(E) + A(E))\,d(E)$$

$$RFe2 := \begin{cases} \exp\left(\frac{-30}{23.4268}\right)\cdot YFe(0.5) & \text{if } Ek \le 1 \le EporFe \\ 0 & \text{otherwise} \end{cases}$$

$$RFe := RFe1 + RFe2$$

$$RFe = 1.821$$

$$\Gamma kFe := \nu kFe\cdot Qi\cdot\left(1 + \frac{dk}{\lambda i}\right)\cdot RFe \qquad \Gamma kFe = 1.292\times 10^{19} \quad cm^{-2}\cdot s^{-1}$$

for As

$$YAs(E) := \frac{5.2\cdot zAs}{EcbAs\cdot\left(zAr^{\frac{2}{3}} + zAs^{\frac{2}{3}}\right)^{\frac{3}{4}}}\cdot\left(\frac{zAr}{zAr + zAs}\right)^{0.67}\cdot\left(\frac{E}{1.4}\right)^{\frac{1}{2}}$$

$$RAs := \int_{Ek}^{EporAs} YAs(E)\cdot(I(E) + A(E))\,d(E)$$

$$RAs1 := \int_{Ek}^{EporAs} YAs(E)\cdot(I\_1(E) + A(E))\,d(E)$$

$$RAs2 := \begin{cases} \exp\left(\frac{-30}{23.4268}\right)\cdot YAs(0.5) & \text{if } Ek \le 1 \le EporAs \\ 0 & \text{otherwise} \end{cases}$$

$$RAs := RAs1 + RAs2$$

$$RAs = 0.856$$

$$\Gamma kAs := \nu kAs\cdot Qi\cdot\left(1 + \frac{dk}{\lambda i}\right)\cdot RAs \qquad \Gamma kAs = 6.075\times 10^{18} \quad cm^{-2}\cdot s^{-1}$$

Determing integral density

$$\Gamma sum := \Gamma kSm + \Gamma kFe + \Gamma kAs \qquad \Gamma sum = 3.105\times 10^{19} \quad cm^{-2}\cdot s^{-1}$$

3. Transfer of sputtered atoms and atomic groups, knocked out of the target to the substrate

Determining average number of collisions of sputtered atoms

for Sm

$$kSm := 2 \cdot \frac{mAr \cdot mSm}{(mAr + mSm)^2}$$

$$kSm = 0.331$$

$$EAr := 1.38 \cdot 10^{-23} \cdot \frac{Temp}{1.67 \cdot 10^{-19}}$$

$$EAr = 0.072 \quad eV$$

$$NkSm := \frac{\log\left(\frac{EAr}{1.22 \cdot EcbSm}\right)}{\log(1 - kSm)}$$

$$NkSm = 11.304$$

for Fe

$$kFe := 2 \cdot \frac{mAr \cdot mFe}{(mAr + mFe)^2}$$

$$kFe = 0.486$$

$$NkFe := \frac{\log\left(\frac{EAr}{EcbFe \cdot 1.22}\right)}{\log(1 - kFe)}$$

$$NkFe = 6.437$$

For As

$$kAs := 2 \cdot \frac{mAr \cdot mAs}{(mAr + mAs)^2}$$

$$kAs = 0.454$$

$$NkAs := \frac{\log\left(\frac{EAr}{EcbAs \cdot 1.22}\right)}{\log(1 - kAs)}$$

$$NkAs = 8.456$$

Determining mean free path of sputtered atoms

$$TempSm := 2350 \quad K$$

$TempFe := 2026 \quad K$

$TempAs := 1703 \quad K$

for Sm

$$\lambda kSm := \frac{4 \cdot 1.38 \cdot 10^{-23} \cdot TempSm}{3.14 \left(\delta kSm \cdot 10^{-10} + \delta aAr \cdot 10^{-10} \right)^2 \cdot p \cdot \left(1 + \frac{mSm}{mAr} \right)^{\frac{1}{2}}}$$

$\lambda kSm = 5.847 \times 10^{-3} \quad m$

for Fe

$$\lambda kFe := \frac{4 \cdot 1.38 \cdot 10^{-23} \cdot TempFe}{3.14 \left(\delta kFe \cdot 10^{-10} + \delta aAr \cdot 10^{-10} \right)^2 \cdot p \cdot \left(1 + \frac{mFe}{mAr} \right)^{\frac{1}{2}}}$$

$\lambda kFe = 9.055 \times 10^{-3} \quad m$

for As

$$\lambda kAs := \frac{4 \cdot 1.38 \cdot 10^{-23} \cdot TempAs}{3.14 \left(\delta kAs \cdot 10^{-10} + \delta aAr \cdot 10^{-10} \right)^2 \cdot p \cdot \left(1 + \frac{mAs}{mAr} \right)^{\frac{1}{2}}}$$

$\lambda kAs = 8.061 \times 10^{-3} \quad m$

Determining average length of the directed motion of atoms to a state of thermalization

$d := 0.080$

for Sm

$LkSm := \lambda kSm \cdot NkSm$

$LkSm = 0.066 \quad m$

for Fe

$LkFe := \lambda kFe \cdot NkFe$

$LkFe = 0.058 \quad m$

for As

$LkAs := \lambda kAs \cdot NkAs$

$LkAs = 0.068 \quad m$

4. Absorption, condensation, formation of the film

Determing the density of the total flow and the velocity of the condensed material

$YSm(0.5) = 1.225$ $\quad YkSm := 1.225$

$YFe(0.5) = 1.312$ $\quad YkFe := 1.312$

$YAs(0.5) = 0.617$ $\quad YkAs := 0.617$

$$Sz := 3 \cdot 10^{-2}$$

$$v := 6 \cdot 10^{-11} \cdot Sz \cdot j \cdot \left[\frac{\nu kSm \cdot YkSm \lambda kSm}{\lambda kSm + \left(\sqrt{d} - \sqrt{LkSm}\right)^2} + \frac{\nu kFe \cdot YkFe \lambda kFe}{\lambda kFe + \left(\sqrt{d} - \sqrt{LkFe}\right)^2} + \frac{\nu kAs \cdot YkAs \cdot \lambda kAs}{\lambda kAs + \left(\sqrt{d} - \sqrt{LkAs}\right)^2} \right]$$

$$v = 6.268 \times 10^{-12} \quad \frac{m}{s}$$

Determining partial flux density of sputtered

$$\Gamma kdSm := \frac{\nu kSm \cdot j \cdot RSm}{el \cdot (1 + \gamma)} \cdot \left(1 + \frac{dk}{\lambda i}\right) \cdot \frac{\lambda kSm}{\left[\lambda kSm + \left(\sqrt{d} - \sqrt{LkSm}\right)^2\right]}$$

$$\Gamma kdSm = 1.083 \times 10^{19} \quad cm^{-2} \cdot s^{-1}$$

$$\Gamma kdFe := \frac{\nu kFe \cdot j \cdot RFe}{el \cdot (1 + \gamma)} \cdot \left(1 + \frac{dk}{\lambda i}\right) \cdot \frac{\lambda kFe}{\left[\lambda kFe + \left(\sqrt{d} - \sqrt{LkFe}\right)^2\right]}$$

$$\Gamma kdFe = 1.086 \times 10^{19} \quad cm^{-2} \cdot s^{-1}$$

$$\Gamma kdAs := \frac{\nu kAs \cdot j \cdot RAs}{el \cdot (1 + \gamma)} \cdot \left(1 + \frac{dk}{\lambda i}\right) \cdot \frac{\lambda kAs}{\left[\lambda kAs + \left(\sqrt{d} - \sqrt{LkAs}\right)^2\right]}$$

$$\Gamma kdAs = 5.738 \times 10^{18} \quad cm^{-2} \cdot s^{-1}$$

Appendix 2

Algorithm for cuprate superconductor $YBa_2Cu_3O_{7-\delta}$

Characterization of the superconductor and the physical parameters of the MSS

1. Specify basic parameters of the components of the superconducting material

Initial physical quantities for calculating the parameters of film deposition

Y	Ba	Cu	O	Ar	
$\nu kY := 0.083$	$\nu kBa := 0.1667$	$\nu kCu := 0.24967$	$\nu kO := 0.6$		gram atomic stoichiometric ratio
$\delta kY := 1.86$	$\delta kBa := 2.7$	$\delta kCu := 1.44$	$\delta kO := 2.8$	$\delta aAr := 3.76$	atom's diameter, A cations
$EcbY := 4.3$	$EcbBa := 1.9$	$EcbCu := 3.5$	$EcbO := 13.61$		connection energy, eV/at
$zY := 39$	$zBa := 56$	$zCu := 29$	$zO := 8$	$zAr := 18$	serial number
$mY := 88.9$	$mBa := 137.3$	$mCu := 53.5$		$mAr := 39.949$	atomic weight, gr/mol

2. Specify basic parameters of the MSS

$Uk := 0.5$	kV	cathode voltage
$j := 5$	$\frac{mA}{cm^2}$	discharge current density
$p := 10$	Pa	pressure of working gas

Modeling basic processes in the "target-substrate" region

1. Creation of the flow of charged and accelerated particles that bombard the target.

The thickness of the near-cathode space:

$$dk := \left(2 \cdot 10^{-2} \cdot \frac{Uk^3}{j^2 \cdot p}\right)^{\frac{1}{5}}$$

$dk = 0.1$ cm

$dk := 0.001$ m

Determing the density of the ion flux Qi

$el := 1.67 \cdot 10^{-19}$ C electron charge

$\gamma := 0.1$ coefficient of electron-ion emission

$$Qi := \frac{j}{el \cdot (1 + \gamma)}$$

$Qi = 2.722 \times 10^{19}$ $cm^{-2} \cdot s^{-1}$

Determing the total flux of atoms and ions Qsum

$k := 1.38 \cdot 10^{-23}$ $\frac{J}{K}$ Bolzman coefficient

$Temp := 873 \quad K$ temperature

$$\lambda i := \frac{4 \cdot k \cdot Temp}{p \cdot \left(\delta aAr \cdot 10^{-10}\right)^2}$$

$\lambda i := 23.426891 0^{-3} \quad m$

$$Qsum := Qi \cdot \left(1 + \frac{dk}{\lambda i}\right)$$

$Qsum = 2.838 \times 10^{19} \quad cm^{-2} \cdot s^{-1}$

2. Sputtering target under the influence of the accelerated flow of energetic particles

Calculating the sputtering glow discharge

$Ek := el \cdot Uk$

$Ek := 0.5 \quad eV$ energy, corresponding to the voltage, applied to the target

for Y

$$\chi Y := \frac{mAr \cdot mY}{(mAr + mY)^2} \qquad EporY := \frac{EcbY}{2 \cdot \chi Y}$$

$EporY = 10.051 \quad eV$

for Ba

$$\chi Ba := \frac{mAr \cdot mBa}{(mAr + mBa)^2}$$

$$EporBa := \frac{EcbBa}{2 \cdot \chi Ba}$$

$EporBa = 5.441 \quad eV$

for Cu

$$\chi Cu := \frac{mAr \cdot mCu}{(mAr + mCu)^2}$$

$$EporCu := \frac{EcbCu}{2 \cdot \chi Cu}$$

$EporCu = 7.15 \quad eV$

Determing the integral energy distribution of ions in the target plane

$$c := 1 + 0.5\left(\gamma^{\frac{-1}{2}} - 1\right)$$

$$h(x) := 1 - \frac{x}{c} - \left(1 - c^{-1}\right) \cdot x^2$$

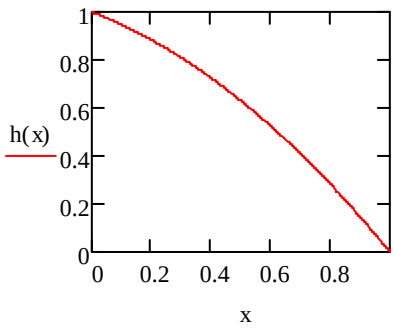

Calculating the integrated effective sputtering coefficient and partial density of atomized flux

for Y

$$YY(E) := \frac{5.2 \cdot zY}{EcbY \cdot \left(zAr^{\frac{2}{3}} + zY^{\frac{2}{3}}\right)^{\frac{3}{4}}} \cdot \left(\frac{zAr}{zAr + zY}\right)^{0.67} \cdot \left(\frac{E}{1.4}\right)^{\frac{1}{2}}$$

$EporY = 10.051 \quad eV$

$elUk := 1 \quad eV$

$eU := 0, 10^{-2} .. 1$

$$I(E) := \frac{1.2}{23.4268} \cdot \exp\left(\frac{-10 \cdot E}{23.4268 \cdot elUk}\right) + \exp\left(\frac{-12}{23.4268}\right) \delta(E - 1)$$

$$I\_1(E) := \frac{30}{23.4268} \cdot \exp\left(\frac{-30 \cdot E}{23.4268 \cdot elUk}\right) + 0$$

$$I\_2(E) := 0 + \exp\left(\frac{-30}{23.4268}\right) \delta(eU - 1)$$

$$hk := \left(\frac{1.67 \cdot 10^{-19} \cdot \lambda i}{mAr \cdot 1.67 \cdot 10^{-27}}\right)^{\frac{2}{5}} \cdot \left[4 \cdot 8.85 \cdot 10^{-12} (1 + \gamma)\right]^{\frac{2}{5}} \cdot \frac{\left(Uk \cdot 10^3\right)^{\frac{3}{5}}}{\left(j \cdot 10^1\right)^{\frac{2}{5}} \cdot p^{\frac{1}{5}}}$$

$hk = 0.03$

$$A(E) := \left(\frac{30}{23.4268} \exp\left(\frac{-30E}{23.4268 \cdot elUk}\right)\right) \cdot \left[1 + \frac{30}{23.4268} \cdot \left(1 - \frac{E}{elUk}\right)\right]$$

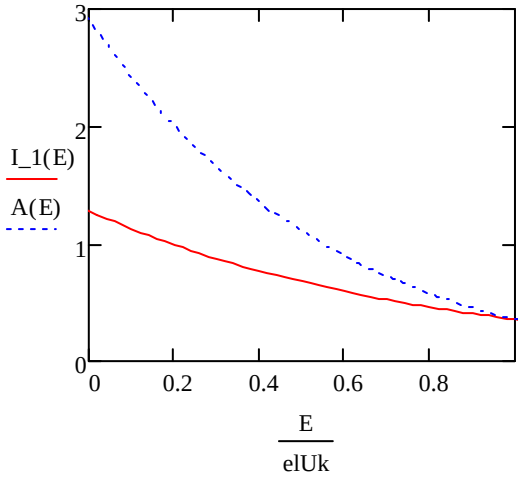

$$RY := \int_{Ek}^{EporY} YY(E)\cdot(I(E) + A(E))\, d(E)$$

$$RY1 := \int_{Ek}^{EporY} YY(E)\cdot(I\_1(E) + A(E))\, d(E) \qquad RY1 = 1.628$$

$$RY2 := \begin{cases} \exp\left(\frac{-30}{23.4268}\right)\cdot YY(0.5) & \text{if } Ek \le 1 \le EporY \\ 0 & \text{otherwise} \end{cases} \qquad RY2 = 0.408$$

$RY := RY1 + RY2$

$$\Gamma kY := \nu kY\cdot Qi\cdot\left(1 + \frac{dk}{\lambda i}\right)\cdot RY$$

$\Gamma kY = 4.796\times 10^{18}$

for Ba

$$YBa(E) := \frac{5.2\cdot zBa}{EcbBa\cdot\left(zAr^{\frac{2}{3}} + zBa^{\frac{2}{3}}\right)^{\frac{3}{4}}}\cdot\left(\frac{zAr}{zAr + zBa}\right)^{0.67}\cdot\left(\frac{E}{1.4}\right)^{\frac{1}{2}}$$

$$RBa := \int_{Ek}^{EporBa} YBa(E)\cdot(I(E) + A(E))\, d(E)$$

$$RBa1 := \int_{Ek}^{EporBa} YBa(E)\cdot(I\_1(E) + A(E))\, d(E)$$

$$RBa2 := \begin{cases} \exp\left(\frac{-30}{23.4268}\right) \cdot YBa(0.5) & \text{if } Ek \le 1 \le EporBa \\ 0 & \text{otherwise} \end{cases}$$

$$RBa := RBa1 + RBa2$$

$$RBa = 4.991$$

$$\Gamma kBa := \nu kBa \cdot Qi \cdot \left(1 + \frac{dk}{\lambda i}\right) \cdot RBa \qquad \Gamma kBa = 2.361 \times 10^{19} \quad cm^{-2} \cdot s^{-1}$$

for Cu

$$YCu(E) := \frac{5.2 \cdot zCu}{EcbCu \cdot \left(zAr^{\frac{2}{3}} + zCu^{\frac{2}{3}}\right)^{\frac{3}{4}}} \cdot \left(\frac{zAr}{zAr + zCu}\right)^{0.67} \cdot \left(\frac{E}{1.4}\right)^{\frac{1}{2}}$$

$$RCu := \int_{Ek}^{EporCu} YCu(E) \cdot (I(E) + A(E))\, d(E)$$

$$RCu1 := \int_{Ek}^{EporCu} YCu(E) \cdot (I\_1(E) + A(E))\, d(E)$$

$$RCu2 := \begin{cases} \exp\left(\frac{-30}{23.4268}\right) \cdot YCu(0.5) & \text{if } Ek \le 1 \le EporCu \\ 0 & \text{otherwise} \end{cases}$$

$$RCu := RCu1 + RCu2$$

$$RCu = 2.319$$

$$\Gamma kCu := \nu kCu \cdot Qi \cdot \left(1 + \frac{dk}{\lambda i}\right) \cdot RCu$$

$$\Gamma kCu = 1.643 \times 10^{19} \quad cm^{-2} \cdot s^{-1}$$

Determining integral density

$$\Gamma sum := \Gamma kBa + \Gamma kY + \Gamma kCu$$

$$\Gamma sum = 4.484 \times 10^{19} \quad cm^{-2} \cdot s^{-1}$$

3. Transfer of sputtered atoms and atomic groups, knocked out of the target to the substrate

Determining average number of collisions of sputtered atoms
for Ba

$$kBa := 2\cdot\frac{mAr\cdot mBa}{(mAr + mBa)^2}$$

$$kBa = 0.349$$

$$EAr := 1.38\cdot 10^{-23}\cdot\frac{Temp}{1.67\cdot 10^{-19}}$$

$$NkBa := \frac{\log\left(\frac{EAr}{2.32}\right)}{\log(1 - kBa)}$$

$$NkBa = 8.081$$

for Y

$$kY := 2\cdot\frac{mAr\cdot mY}{(mAr + mY)^2}$$

$$kY = 0.428$$

$$EAr = 0.072$$

$$NkY := \frac{\log\left(\frac{EAr}{EcbY\cdot 1.22}\right)}{\log(1 - kY)}$$

$$NkY = 7.678$$

for Cu

$$kCu := 2\cdot\frac{mAr\cdot mCu}{(mAr + mCu)^2} \qquad kCu = 0.489$$

$$NkCu := \frac{\log\left(\frac{EAr}{EcbCu\cdot 1.22}\right)}{\log(1 - kCu)} \qquad NkCu = 6.07$$

Determining mean free path of sputtered atoms

$$TempBa := 2350 \quad K$$

$$TempY := 2026 \quad K$$

$$TempCu := 1703 \quad K$$

for Ba

$$\lambda kBa := \frac{4\cdot 1.38\cdot 10^{-23}\cdot TempBa}{3.14\left(\delta kBa\cdot 10^{-10} + \delta aAr\cdot 10^{-10}\right)^2\cdot p\cdot\left(1 + \frac{mBa}{mAr}\right)^{\frac{1}{2}}}$$

$$\lambda kBa = 4.7\times 10^{-3} \quad m$$

for Y

$$\lambda kY := \frac{4 \cdot 1.38 \cdot 10^{-23} \cdot TempY}{3.14 \cdot \left(\delta kY \cdot 10^{-10} + \delta aAr \cdot 10^{-10}\right)^2 \cdot p \cdot \left(1 + \frac{mY}{mAr}\right)^{\frac{1}{2}}}$$

$\lambda kY = 6.279 \times 10^{-3}$ m

for Cu

$$\lambda kCu := \frac{4 \cdot 1.38 \cdot 10^{-23} \cdot TempCu}{3.14 \cdot \left(\delta kCu \cdot 10^{-10} + \delta aAr \cdot 10^{-10}\right)^2 \cdot p \cdot \left(1 + \frac{mCu}{mAr}\right)^{\frac{1}{2}}}$$

$\lambda kCu = 7.239 \times 10^{-3}$ m

Determining average length of the directed motion of atoms to a state of thermalization

for Ba

$LkBa := \lambda kBa \cdot NkBa$

$LkBa = 0.038$ m

for Y

$LkY := \lambda kY \cdot NkY$

$LkY = 0.048$ m

for Cu

$LkCu := \lambda kCu \cdot NkCu$ $LkCu = 0.044$ m

4. Absorption, condensation, formation of the film

Determining density of the total flow and the velocity of the condenced material

$YBa(0.5) = 3.557$ $YkBa := 4.209$

$YY(0.5) = 1.467$ $YkY := 1.736$

$YCu(0.5) = 1.668$ $YkCu := 1.974$

$d := 0.060$

$$Sz := 3 \cdot 10^{-2}$$

$$v := 6 \cdot 10^{-11} \cdot Sz \cdot j \cdot \left[\frac{\nu kBa \cdot YkBa \cdot \lambda kBa}{\lambda kBa + \left(\sqrt{d} - \sqrt{LkBa}\right)^2} + \frac{\nu kY \cdot YkY \cdot \lambda kY}{\lambda kY + \left(\sqrt{d} - \sqrt{LkY}\right)^2} + \frac{\nu kCu \cdot YkCu \cdot \lambda kCu}{\lambda kCu + \left(\sqrt{d} - \sqrt{LkCu}\right)^2} \right]$$

$$v = 9.077 \times 10^{-12} \quad \frac{m}{s}$$

$$\Gamma kdY := \frac{\nu kY \cdot j \cdot RY}{el \cdot (1 + \gamma)} \cdot \left(1 + \frac{dk}{\lambda i}\right) \cdot \frac{\lambda kY}{\left[\lambda kY + \left(\sqrt{d} - \sqrt{LkY}\right)^2\right]}$$

$$\Gamma kdY = 4.35 \times 10^{18} \quad cm^{-2} \cdot s^{-1}$$

$$\Gamma kdBa := \frac{\nu kBa \cdot j \cdot RBa}{el \cdot (1 + \gamma)} \cdot \left(1 + \frac{dk}{\lambda i}\right) \cdot \frac{\lambda kBa}{\left[\lambda kBa + \left(\sqrt{d} - \sqrt{LkBa}\right)^2\right]}$$

$$\Gamma kdBa = 1.54 \times 10^{19} \quad cm^{-2} \cdot s^{-1}$$

$$\Gamma kdCu := \frac{\nu kCu \cdot j \cdot RCu}{el \cdot (1 + \gamma)} \cdot \left(1 + \frac{dk}{\lambda i}\right) \cdot \frac{\lambda kCu}{\left[\lambda kCu + \left(\sqrt{d} - \sqrt{LkCu}\right)^2\right]}$$

$$\Gamma kdCu = 1.401 \times 10^{19} \quad cm^{-2} \cdot s^{-1}$$